UNIVERZITY OF HRADEC KRÁLOVÉ

FACULTY OF INFORMATICS AND MANAGEMENT

DEPARTMENT OF INFORMATION TECHNOLOGY

DISSERTATION

Optimization of processing and classification of signal data using convolutional neural networks

Subject: Applied Informatics

Author: Ing. Dalibor Cimr

Supervisor: Assoc. Prof. Ing. Bc. Hana Tomášková, Ph.D.

Hradec Králové April 2023

Declaration:

I certify that I wrote the dissertation independently and that I included a list of all sources used in the bibliography.

In Hradec Králové Ing. Dalibor Cimr

Acknowledgement:

I want to express my gratitude to Assoc. Prof. Hana Tomášková, PhD, for her willingness to lead this dissertation. Additionally, I'd like to express my gratitude to everyone who encouraged me to complete this study.

Contents

List of abbreviations

Acc	accuracy
AFDB	MIT-BIH atrial fibrillation database
A_{fib}	atrial fibrillation
A_{fl}	atrial flutter
ALE	accumulated local effects
ANOVA	analysis of variance
AUC	area under curve
AVN	atrioventicular node
BCG	balistocardiography
CAD	computer aided detection
CNN	convolutional neural network
CUDB	Creighton University Ventricular Tachyarrhythmia Database
CWT	continuous wavelet transform
DT	decision tree
DWT	discrete wavelet transform
ECG	electrocardiogram

EDB	European ST-T Database
EEG	electroencephalogram
EMD	empirical mode decomposition
FN	false negative
FP	false positive
GAN	generative adversarial network
KNN	k-nearest neighbor
LDA	linear discriminant analysis
LIME	local interpretable model-agnostic explanations
MITDB	MIT-BIH arrhythmia database
NN	neural network
NSRDB	MIT-BIH Normal Sinus Rhythm Database
PD	partial dependence
PPG	photoplethysmogram
PPV	positive predicted value
ReLU	rectifier linear unit
RF	random forest
RNN	recurrent neural network
RQA	recurrence quantification analysis
Sen	sensitivity
Spec	specificity
STFT	short-time Fourier transform
SVM	support vector machine

TN	true negative
TP	true positive
VFDB	MIT-BIH malignant ventricular arrhythmia database
$\mathbf{V_{fib}}$	ventricular fibrillation

List of Figures

List of Tables

Abstract

The doctoral thesis focuses on increasing the efficiency of signal data processing and classification using convolutional neural networks. The topic is divided into three significant sub-areas: data processing, data fusion, and model architecture analysis. The thesis covers the literature on signal processing and classification that leads to cutting-edge approaches and their time consumption gaps.

The main building blocks of the proposed work are freely available datasets from several healthcare sectors, their preprocessing, fusion, and classification. In all of these domains, the thesis accomplishes findings, compares them to current methodologies in the literature, and explains the differences. With appropriate precision for application, the suggested approach for signal classification outperforms the complexity of existing papers.

Keywords:

CNN, CAD, data processing, data fusion, EEG, ECG, BCG

Anotace

Disertační práce se zaměřuje na zvýšení efektivity zpracování a klasifikace signálových dat pomocí konvolučních neuronových sítí. Téma je rozděleno do tří významných podoblastí: zpracování dat, fúze dat a analýza architektury modelu. Práce zahrnuje literaturu o zpracování a klasifikaci signálů, která vede ke špičkovým přístupům a jejich nedostatkům v rychlosti výpočtů.

Hlavními stavebními bloky navrhované práce jsou volně dostupné datové soubory z několika odvětví zdravotnictví, jejich předzpracování, fúze a klasifikace. Ve všech těchto oblastech práce naplňuje poznatky, porovnává je se současnými metodikami v literatuře a vysvětluje rozdíly. S náležitou přesností pro aplikaci navrhovaný přístup ke klasifikaci signálů překonává složitost stávajících prací.

Keywords:

CNN, CAD, zpracování dat, fúze dat, EEG, ECG, BCG

1

Introduction

Machine learning research has gained significant popularity in recent years due to advancements in technology and performance. These improvements have enabled solving increasingly complex issues that were previously impossible to calculate within a reasonable timeframe. This has led to the development of more sophisticated models and systems for classifying and detecting problems. One of the most notable areas where machine learning has significantly impacted image processing. With the use of two-dimensional equipment, three-dimensional objects can now be scanned, and their diversity in terms of position, size, color, shape, and other features can be identified and solved.

Despite the technological advances in machine learning, there are still areas where it is appropriate to explore the possibilities of system optimization for lower computational demands without compromising performance. One such area is the classification of vital healthcare data. Medical health analysis devices typically measure data in vectors or sets of vectors, which are then sampled to an appropriate form. Based on this data, machine learning algorithms can be used as decision support systems to detect health issues. The key benefit of such systems is that they allow for continuous monitoring of patient conditions, saving time for medical professionals in hospitals or carers at home. Early signaling is critical in the event of therapy, and such systems are referred to as computer aided detection (CAD).

CAD systems offer several benefits in the field of healthcare. In addition to saving time for medical professionals, CAD systems can reduce the likelihood of human error, especially when detecting complex patterns. These systems can also detect health issues that might not be immediately apparent to medical professionals, allowing for early intervention and potentially better patient outcomes. However, CAD systems are not without limitations. For example, they may not be able to detect certain health issues, and false positives can

sometimes occur. Therefore, CAD systems should be used as decision support tools and not as a substitute for medical professionals.

During the research, it is essential to evaluate not only the quality of the models but also their deployment possibilities. This is particularly important in the healthcare industry, where the availability and application of modern approaches are necessary, even in the absence of cutting-edge hardware. The healthcare industry is constantly evolving, with the adoption of modern technologies playing a significant role in its progress. However, the high cost of modern hardware can pose significant financial constraints, making it challenging to provide quality healthcare services. Therefore, exploring alternative methods to improve healthcare services and make them more accessible to everyone is necessary. Hence, exploring alternative methods to provide quality healthcare services is necessary.

One of the popular machine learning techniques used in various industries is convolutional neural network (CNN). This technique was designed initially for image classification and detection but has since been applied in other fields. CNN is a feed-forward neural network extended by convolution operations to improve classification performance. To improve the efficiency of the CNN architecture, this thesis focuses on a literature review of existing approaches and identifies potential improvements in computational complexity. Additionally, experiments will be conducted to analyze the efficiency increase.

The thesis presents a methodology based on long-term research focused on various health issue databases. The first approach was made using electrocardiogram (ECG) databases and was published in articles [32, 33]. The subsequent research involved working with balistocardiography (BCG) data and was presented in papers [21–23]. The last part of the study was focused on seizure detection from electroencephalogram (EEG) signals and is presented in article [24]. Experiments were performed in reverse on datasets from older publications to confirm the evaluations from articles.

The proposed solution's flowchart is illustrated in Figure 1.1. The first step involves loading the data from databases that are briefed in subsection 3.3 to conduct experiments on health issues described in subsection 3.2. The following part involves preparing the raw data into a suitable form, which is discussed in section 3.4, with the results presented in section 4.1. In the case of multi-channel data, channel fusion is provided, and the motivation for the proposed solution is discussed in section 3.5, with experiments presented in section 4.2. The third part of the system deals with frequency analysis, with theory and hypothesis presented

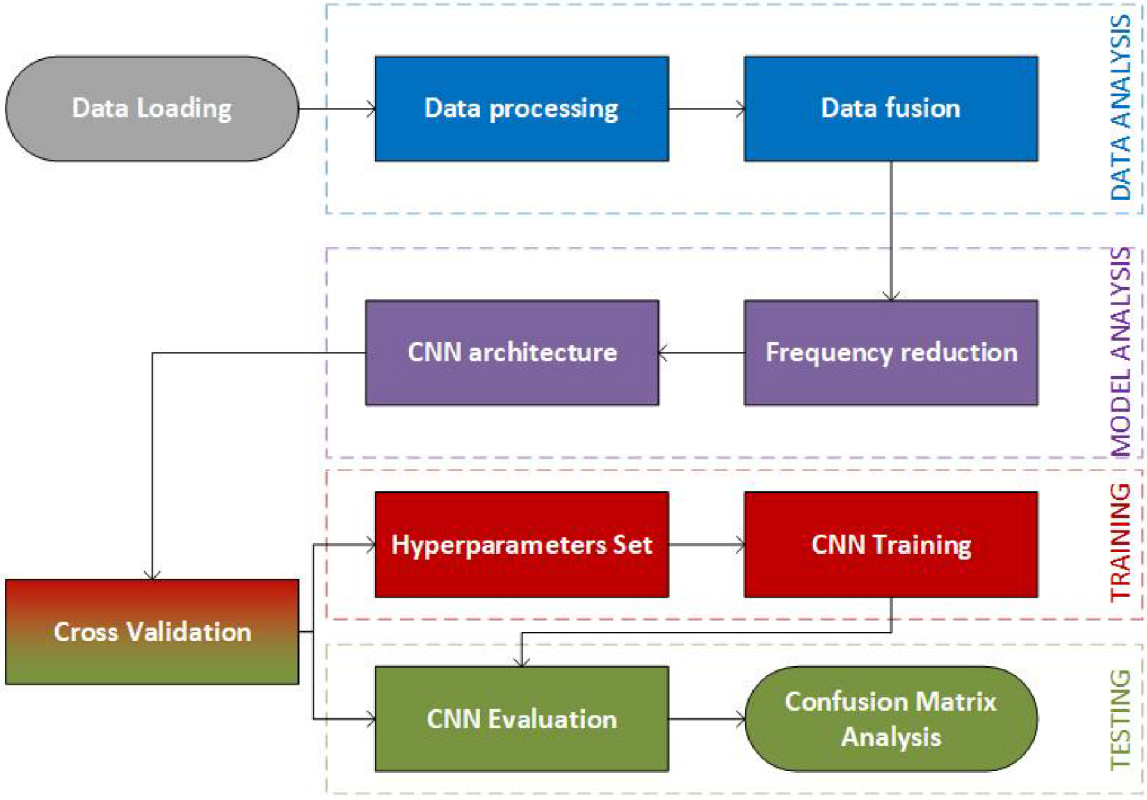

Figure 1.1: Flowchart diagram of the system [created by the author]

in section 3.6, and evaluation in section 4.3, together with an analysis of the architecture. The training and testing tasks were carried out with two CNN architectures using common experiment settings from section 3.1. Since the thesis is divided into numerous submodules, each portion's discussion is presented with the results in the same section to improve text readability and comprehension.

2

The work's objectives

This dissertation aims to suggest improving the computer processing of signal data for proper categorization in informatics. These enhancements will be evaluated and illustrated using signal data from a hospital setting. One of the most important things is to thoroughly analyze the raw data to extract many crucial components for further target selection. Suitable CNN designs for data classification will be explored, which have lately seen a surge in popularity and are utilized to reduce several typical procedures before data classification itself [5, 32]. The suggested technique will establish an ideal classifier for accuracy and reliability and decrease the computing complexity and time necessary to acquire the classification result.

The dissertation's main goal is to increase the efficiency of the classification system, which is solved by the following objectives:

1. **Data processing**

   CAD systems are often constructed in standard flowchart ways with preprocessing, feature extraction, feature selection, and classification operations. The goal is to investigate the sections in conjunction with the CNN classifier for system reduction by reducing computing time or deleting some processes entirely.

2. **Data fusion**

   Because healthcare involves measuring additional devices or channels, the data fusion procedure was explored to reduce complexity and reliance on utilized channels. With the correct parameters, network architecture may be simplified by one dimension without sacrificing performance to detect health risks.

3. **CNN analysis**

   Model input resolution does not have to be of the best quality regarding picture categorization. The CNN model must discover the major patterns that distinguish

classes. It led to frequency reduction experiments and an architectural evaluation of all healthcare problems by selecting a suitable collection of blocks and filters based on the input shape.

3

Methodology

3.1 Experiments setup and CNN architectures

The work includes several experiments involving various components of the classification system. Despite this diversity, the training and testing processes follow some of the conventional practices commonly used in literature. Furthermore, the experiments employ two design CNN architectures developed in the research.

3.1.1 Training and testing

The dataset is first divided using a stratified ten-fold cross-validation strategy [28] to assess the model's performance. This strategy aims to ensure that the distribution of classes in each fold is representative of the entire dataset. This method divides the data into ten equally large groups, each with a similar proportion of samples for each class.

Nine of the ten groups are used for training and testing to evaluate the model's performance, while the remaining group is held out for validation. Specifically, the training and testing sets are split into 70% and 30% parts, respectively. The training part of the system depends on two main hyperparameters: the number of epochs and the learning rate.

One epoch passes each training sample, followed by validation on testing samples. An epoch is a single pass through the entire training dataset. During training, the model learns to adjust its weights to minimize the difference between its predictions and the true labels of the training data. The validation step evaluates the model's performance on the testing data to detect overfitting, where the model fits the training data too well and cannot generalize to new data.

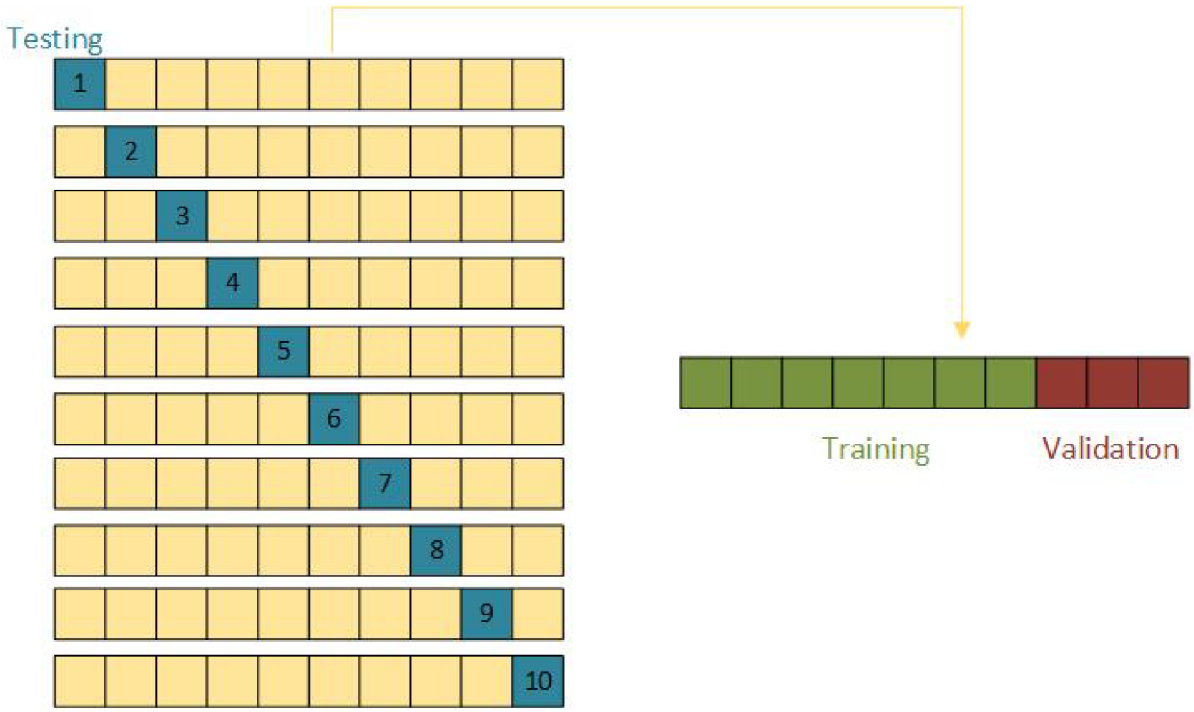

Figure 3.1: Data division process [created by the author]

The learning rate is a crucial hyperparameter determining the weight changes' size during each model update. A low learning rate means the model will take longer to converge to the optimal weights, while a high learning rate can result in large weight changes that overshoot the optimal values. Therefore, the learning rate value does not have to be constant for the entire training process. In this study, we set the learning rate parameter to $1 \cdot 10^{-3}$ for the first 25 epochs, with a dropping factor that varies depending on the number of epochs.

This strategy provides balanced learning of the dataset where the main patterns are recognized in the first part of epochs, and more detailed differences of patterns are learned in the later epochs. The initial learning rate was chosen to be low to ensure that the model's weights are initialized close to their optimal values. At the same time, the dropping factor allows for gradual increases in the learning rate to promote more efficient learning. This approach enables us to assess the model's performance systematically and reliably, which is critical for developing accurate and generalizable machine learning models.

Table 3.1 describes the hyperparameters used in the model training process. One of the key strategies used is the step decay approach, which involves decreasing the learning rate parameter according to a predetermined schedule. Specifically, the learning rate is decreased every 25 epochs by a value of $2 \cdot 10^{-1}$ from its initial value of $1 \cdot 10^{-3}$, using the Adam optimizer. This strategy is based on the appropriate gradient descent techniques

Table 3.1: Hyperparameters used for training the model [created by the author]

Input Size	Optimizer	Learning rate	Learning rate schedule	Learning rate drop	Mini batch size	Epochs
499x1	Adam	1e-3	Step decay	2e-1	32	100

[75]. During the initial stages of the training process, the model focuses on learning the main pattern differences between the different classes. This is followed by fine-tuning the weights and biases of the model to improve its accuracy (Acc) and performance. Another important parameter is the batch size, which determines the number of inputs the model processes before it is updated. In this case, the batch size has been set to 32, considered an appropriate value for this model type. This ensures the model can process sufficient data without being overwhelmed or experiencing memory issues.

The evaluation of classification results to assess the performance of a model is made by confusion matrix, a useful tool for this purpose that allows tabulating the number of true positive (TP), true negative (TN), false positive (FP), and false negative (FN). These metrics are shown in Table 3.2. TP and TN correspond to the correct classification of normal and abnormal signals, respectively. FP and FN represent the wrong decisions made by the model.

When dealing with more than two classes, the normal data encompasses all signals without health problems, and the abnormal data refers to the rest of the dataset. In binary classification, the Acc of the test is a statistical measure of how well it can detect or eliminate a condition. In other words, Acc represents the fraction of correct predictions, including true positives and negatives, among all instances evaluated.

The positive predicted value (PPV) is a proportion of cases with positive test results that are already patients. This measure provides information about the probability of a true positive result when the test is positive. sensitivity (Sen) and specificity (Spec) are two other important metrics used to evaluate the Acc of a test that reports the presence or absence of a disease. The criteria for a positive result are met when an individual is considered "positive", while a "negative" result means that the criteria are not met. Sen, also known as the true positive rate, represents the chance of a positive test result when an individual is positive. On the other hand, Spec, also known as the true negative rate, refers to the likelihood of a negative test result when an individual is negative.

Table 3.2: Confusion matrix description [created by the author]

O/P	Normal	Abnormal	Acc (%)	PPV (%)	Sen (%)	Spec (%)
Normal	TP	FN	$\frac{TP+TN}{TP+TN+FP+FN}$	$\frac{TP}{TP+FP}$	$\frac{TP}{TP+FN}$	$\frac{TN}{TN+FP}$
Ubnormal	FP	TN	$\frac{TP+TN}{TP+TN+FP+FN}$	$\frac{TN}{TN+FN}$	$\frac{TN}{TN+FP}$	$\frac{TP}{TP+FN}$

3.1.2 Architecture 1

CNN consists mainly of convolutional layers and max-pooling layers. The network's order and number of layers can vary and are characterized by their kernel size, which describes the filter's dimensions, the number of filters, and the stride of search.

In the model, the input layer has a resolution of 499x1, and the first layer after it is a convolutional layer with 12 filters and a kernel size of 19. This means the layer performs a convolution operation on the input image using 12 filters of size 19x1. The output of this layer is a feature map, which is then passed through a max-pooling layer with a kernel size of 2. Each pair of values in the feature map is compared in this layer, and the larger value is retained for the next layer. This effectively halves the number of neurons in the feature map, and the number of filters remains the same as in the previous layer.

This convolutional and max-pooling layer sequence is repeated twice in the model. In the second convolutional layer, the kernel size is set to 19, but only 11 filters are used. In the third convolutional layer, 12 filters are used with a kernel size of 11. In both cases, the max-pooling layer has the same kernel size and stride as in the first layer. The stride of convolutional layers is set to 1, and the stride of max-pooling layers is set to 2. After these six layers, the number of output neurons is 550, consisting of 11 vectors with a size of 50.

The next layer of the architecture is fully connected. In this layer, each neuron is connected to every neuron in the previous. Specifically, there are 11 neurons in this layer. The final layer is also fully connected, with four outputs representing the four classes. The whole model is summarized in Table 3.3 and Figure 3.2 and has been created by several experiments and analyses of architecture properties.

Moreover, dropout layers and rectifier linear unit (ReLU) layers address the problem of over-fitting and optimization [83]. The ReLU is an activation function used in all convolutional layers, which introduces non-linearity into the network. The dropout layer is implemented after the first fully connected layer, with a value of 0.3, which means that 30% of the neurons in that layer are randomly dropped out during training.

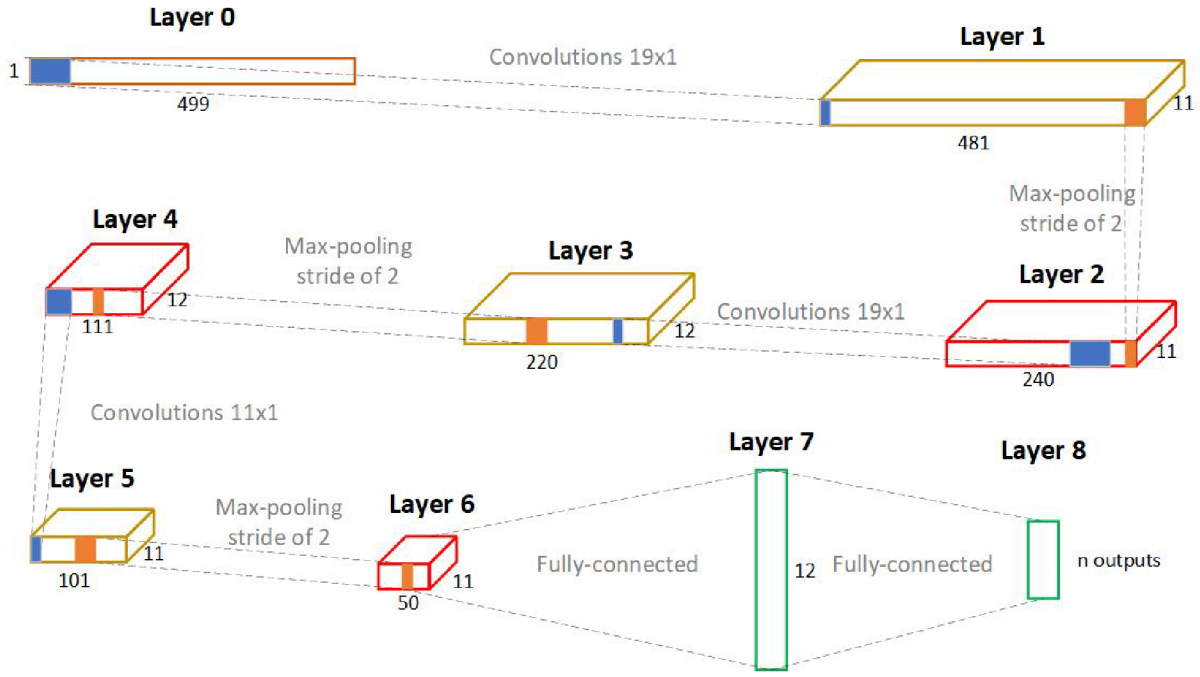

Figure 3.2: The architecture of the proposed CNN model 1 [created by the author]

Table 3.3: The details of CNN structure 1 with n classes depending on classification task [created by the author]

Layers	Type	No. of output neurons	Kernel size	Stride
0-1	convolution	481 x 11	19	1
1-2	max-pooling	240 x 11	2	2
2-3	convolution	220 x 12	19	1
3-4	max-pooling	110 x 12	2	2
4-5	convolution	101 x 11	11	1
5-6	max-pooling	50 x 11	2	2
6-7	fully connected	12	-	-
7-8	fully connected	n	-	-

Additionally, normalization is necessary to obtain suitable results in the network. Our model uses a normalized exponential function called the softmax function as the final layer's activation function. The softmax function ensures that the output values of the network lie between 0 and 1 and sum up to 1, making it easier to interpret the output as probabilities belonging to different classes.

3.1.3 Architecture 2

The second CNN architecture underwent modifications due to a different input shape, as it was designed in a 2-dimensional form in the last paper about disordered breathing

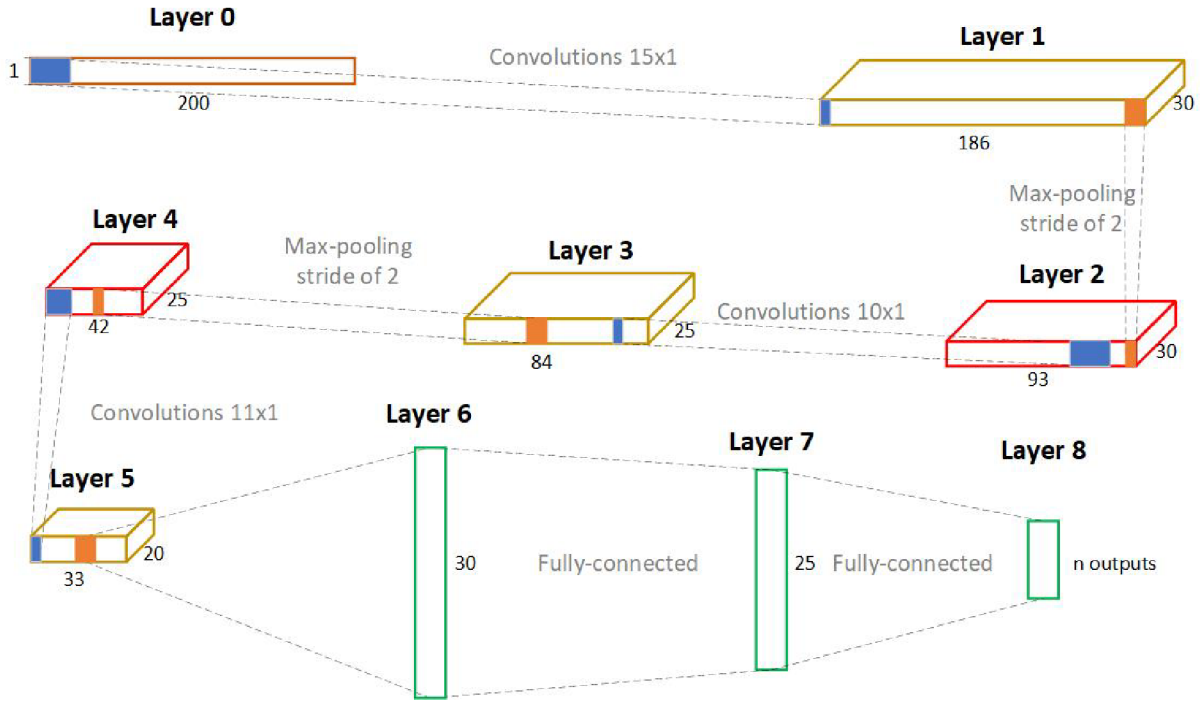

Figure 3.3: The architecture of the proposed CNN model 2 [created by the author]

from BCG [23]. The model was subsequently modified to the proper form to evaluate vector inputs. The architecture presented in this paper is shown in Figure 3.3 and table 3.4.

o reduce the complexity of the architecture, the input to the network is represented by downsampled features from 450 to 200. The first four layers constitute two combinations of convolutional and max-pooling layers. All max-pooling layers have a kernel with a resolution of 2. Due to the resolution of features, the architecture continues with a convolutional layer of kernel size ten without a max-pooling operation. After that, two fully-connected layers, which analyze features from previous layers, are implemented with 30 and 25 neurons, respectively.

The last fully-connected layer with n neurons corresponding to classes predicts the result by a softmax activation function. This function normalizes the result of the architecture to a suitable form on the value between 0 and 1 with a threshold of 0.5 for prediction. Moreover, mechanisms for over-fitting prevention, which have an important impact on the model training process [83], are applied too. Specifically, there are ReLU layers between all convolution and max-pooling layers and a dropout layer with a drop parameter of 0.3 between the first and second fully-connected layers.

Table 3.4: The details of CNN structure 2 with n classes depending on classification task [created by the author]

Layers	Type	No. of output neurons	Kernel size	Stride
0-1	convolution	186 x 30	15	1
1-2	max-pooling	93 x 30	2	2
2-3	convolution	84 x 25	10	1
3-4	max-pooling	42 x 25	2	2
4-5	convolution	33 x 20	10	1
5-6	fully connected	30	-	-
6-7	fully connected	25	-	-
7-8	fully connected	n	-	-

3.2 Health problematics

The research deals with vector data in the health care task and works with various datasets reflecting various health conditions. The following subsections describe what and how the devices measured data and explain what each aberrant class represents in medicine.

3.2.1 Electrocardiography

The ECG operates by measuring the projection of the heart polarization vector [79]. This vector is measured by electrodes placed on the human body in the correct position, depending on the number of electrodes used. While it is possible to use only two electrodes, using three electrodes provides a better signal-to-noise ratio. More than three are used for measuring different projections of the polarization vector [95]. This measurement is vital in the diagnosis and monitoring of various heart conditions.

Exploration of cardiac activity is based on the search for unambiguous patterns that describe beat-to-beat processes. These processes are called T wave, P wave, and QRS complex [61]. P and T waves represent the depolarization and repolarization of the atria. The P wave occurs before the QRS complex, while the T wave occurs after. On the other hand, the QRS complex represents the depolarization of the heart chambers. QRS complex detection is one of the basic approaches used for detecting abnormal heart behaviour, and it is used extensively in ECG analysis [99].

Arrhythmias and flutters are common heart diseases characterized by abnormal heart rhythms. The prevalence of these conditions is high, and there is a constant increase in the number of cases detected in the population. These diseases fall under the category of heart

arrhythmias, which affect a higher percentage of males in the population, and the elderly population is predominantly affected [20, 25, 86].

The most occurring type of arrhythmia is called atrial fibrillation (A_{fib}) manifested by the absence of repeating P waves [48] and uncoordinated atrial activation due to the behaving of the atrioventicular node (AVN) [53].The AVN reacts to signals with a precise intensity, but in the case of A_{fib}, this intensity is disrupted, leading to irregular rhythms. Another atrial illness is atrial flutter (A_{fl}) which does not influence AVN. A_{fl} occurs in a macro reentrant circuit and has a typical underlying electrophysiological mechanism [73]. Although there is evidence of interdependence between atrial fibrillation and atrial flutte A_{fib} and A_{fl} [89, 90], but A_{fl} may have an impact on morbidity and mortality despite the non-attendance of A_{fib}.

The ventricular fibrillation (V_{fib}) is an arrhythmia established in the specialized conduction system or ventricular muscle. It is characterized by the absence of necessary peaks in the sinus process of the measured signal. These peaks represent the correct electromagnetic pulse of the heart [66].

3.2.2 Balistocardiography

BCG is a non-invasive method of sensing body micro-movements evoked by heart activity and blood flow in large arteries. Since the first research of ballistic displacements of the body [37], there has been considerable progress in BCG and ballistocardiography sensors despite a lack of interest in the past because of insufficient knowledge of physiology and physics behind the method [46]. However, recent technological advances, including the development of highly sensitive sensors and fast computers for real-time calculations, have renewed interest in this field of science. Nowadays, physicians mostly work with ECG signals to disclose heart-related health problems of patients [30]. However, it is possible to detect similar and even more information by BCG signals, and unlike the ECG, measurement by BCG is unobtrusive.

Breathing disorders are a prevalent sleep-related issue that affects the entire population regardless of age or gender. The most significant group affected by these disorders are those who suffer from obesity or are overweight. The primary manifestation of these disorders is the collapse of the pharyngeal airway during sleep, which prevents regular breathing. As a result, patients suffer from somnolence, poor daytime cognitive performance, and cardiovascular morbidity and mortality [41].

There are three types of disordered breathing: sleep apnea, central sleep apnea, and nocturnal hypoventilation. Sleep apnea is caused by an obstruction in the upper respiratory tract, but the breathing effort is maintained. On the other hand, central sleep apnea is caused by a central nervous system issue and has no breathing effort. The difference lies in their causation [84]. Nocturnal hypoventilation, the third type of breathing disorder, is characterized by shallow and slowed breathing in which the airflow is insufficient for the body's requirements [67].

3.2.3 Electroencephalography

EEG is a medical diagnostic technique that enables the detection and recording of the electrical activity in the brain using non-invasive or invasive methods [15]. Non-invasive EEG testing is typically performed by attaching electrodes to the scalp to capture the brain's spontaneous activity. The recorded signals are then analyzed to diagnose various neurological and psychiatric conditions. Invasive EEG testing is performed by placing electrodes directly on the brain's surface or within the brain tissue. This method is used when non-invasive testing fails to provide sufficient diagnostic information. The information obtained from EEG testing can be used to operate various medical devices and equipment, including brain-computer interfaces.

Evoked potentials are the brain's responses to external stimuli detected using EEG. Somatosensory potentials are elicited by stimulating peripheral nerves in the upper and lower limbs. Auditory potentials are generated in response to brief noises, while visual potentials are elicited using a reverse checkerboard pattern. The electrical signals recorded from the brain in response to these stimuli are analyzed to assess the integrity of the brain's sensory and motor pathways. The potential to diagnose several neurological conditions, such as multiple sclerosis, optic neuritis, and brainstem lesions.

Epilepsy is a chronic neurological disorder characterized by epileptic seizures [85]. These seizures are sudden episodes of abnormal brain activity that manifest as temporary changes in consciousness, perception, behavior, movement, or sensation. Epilepsy is a common disorder that affects individuals of all ages, genders, and ethnicities worldwide. The exact cause of epilepsy is unknown in most cases, but it may result from brain injuries, infections, genetic factors, or developmental disorders. The diagnosis of epilepsy is primarily based on clinical history, EEG testing, and imaging studies. The treatment of epilepsy involves the

use of antiepileptic drugs, surgery, or a combination of both. The goal of treatment is to reduce or eliminate the occurrence of seizures and improve the quality of life of the affected individuals [97].

3.3 Data description

As specified in the documentation, the databases chosen for this study were evaluated using several parameters, including frequency, number of channels, device type, and data labeling. As a result, various source code implementations were developed to convert the data into the necessary format for analysis. The subsequent subsections provide a detailed description of each of these settings and the data they entail.

3.3.1 Electrocardiography

The ECG samples used in this work were collected from the public PhysioBank database [36], concretely three different databases to obtain the necessary data for the experiments. The first database, known as the MIT-BIH malignant ventricular arrhythmia database (VFDB) provided data on V_{fib}, the MIT-BIH atrial fibrillation database (AFDB) for both A_{fib} and A_{fl}, and the MIT-BIH arrhythmia database (MITDB) contains data on A_{fib}, A_{fl}, V_{fib}, and normal samples. A detailed summary of the ECG databases and the number of samples obtained from each database are provided in Table 3.5.

It is worth noting that these databases are raw data containing no pre-processing or normalization steps. This lack of preprocessing and normalization makes these datasets ideal for our research, as it allows us to analyze and compare the performance of different models under the same conditions. Additionally, the PhysioBank database is frequently used in healthcare research, ensuring that our results are directly comparable to other studies using similar data. The AFDB database includes 25 ECG, each lasting 10 hours, of humans withA_{fib}, mostly paroxysmal. The MITDB contains 48 half-hour excerpts of two-channel ambulatory ECG recordings, which cover all the categories mentioned earlier. Finally, the VFDB includes 22 half-hours ECG recordings of subjects who experienced episodes of sustained V_{fib}. In sum, 25287 inputs to the CNN model with a two-second duration were prepared for experiments. These inputs were created without data overlapping so no section was used more than once.

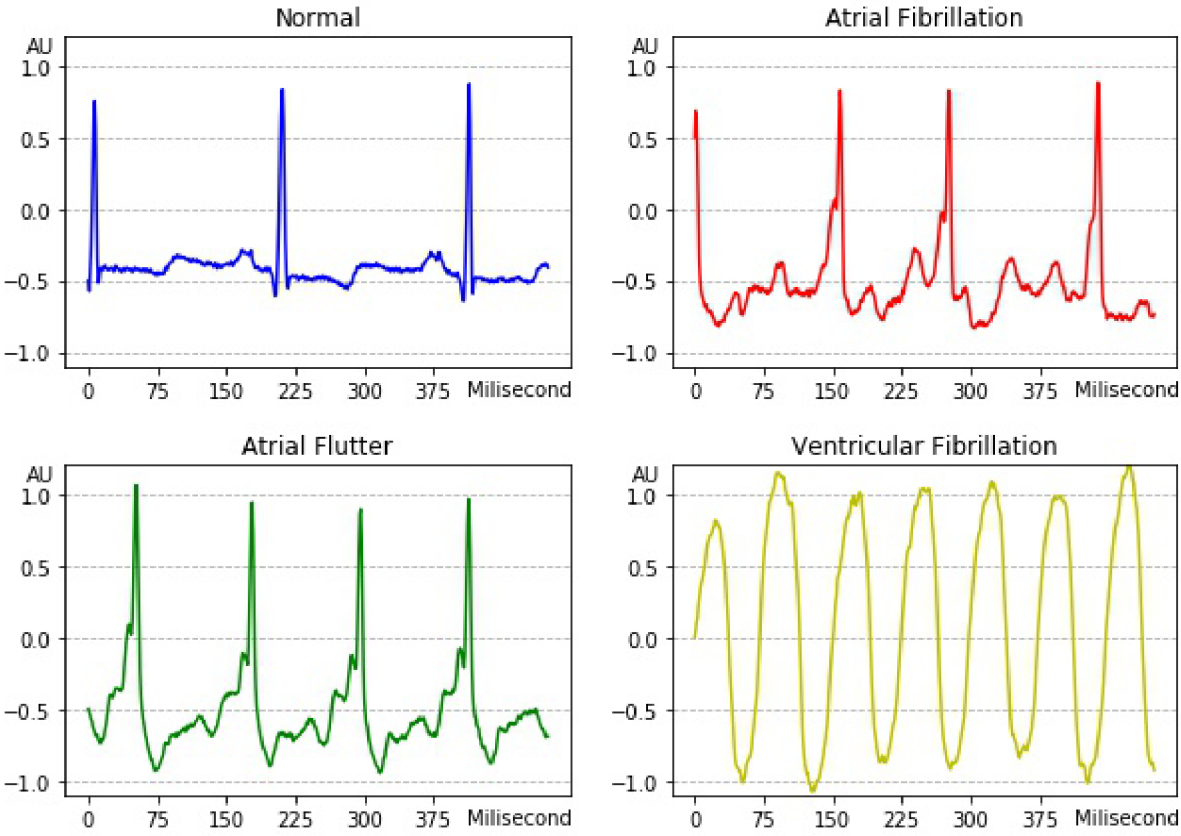

Figure 3.4: An illustration of ECG segments of normal, A_{fib}, A_{fl}, and V_{fib} patterns [32]

Table 3.5: Number of samples overview used from PhysioBank databases for each class [32]

Type	No. of samples	Used databases
N_r	3, 567	MITDB
A_{fib}	19, 276	AFDB, MITDB
A_{fl}	1, 518	AFDB, MITDB
V_{fib}	923	MITDB, VFDB

To better understand the different categories of ECG data obtained from the PhysioBank database, we have included sample examples of all four categories in Figure 3.4. The figure shows representative ECG waveforms from each category, demonstrating the unique features of each category.

3.3.2 Balistocardiography

The BCG samples used in this work were collected from the public Mendeley database [82] and measured in the laboratory of the University of Hradec Kralove. The dataset was obtained from twenty tested individuals, consisting of 11 men aged 23 to 33 years and 9 women aged 24 to 65 years. During the measurements, the subjects were lying on a bed with

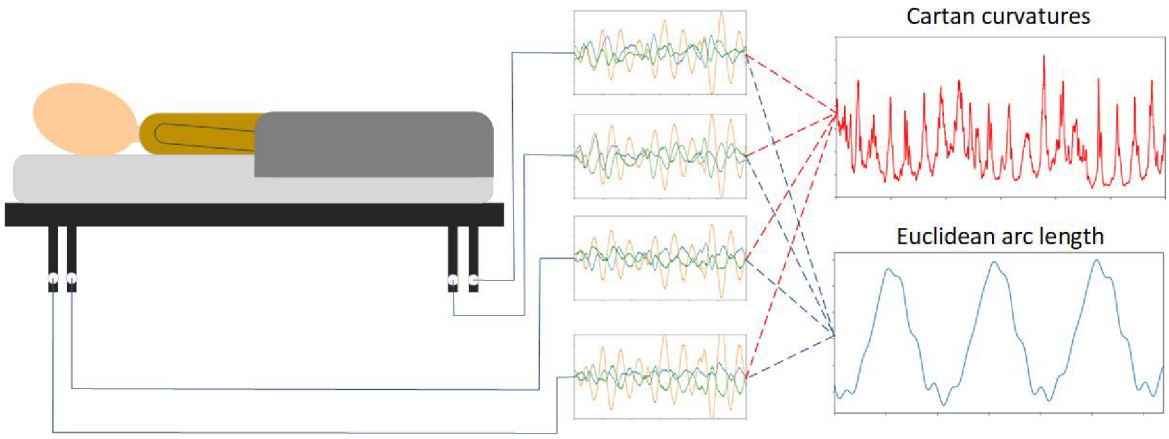

Figure 3.5: BCG Measured force signals (x: time/[ms], y: AU, standardized raw data) [21]

sensors placed on the bed legs, as illustrated in Fig 3.5. Table 3.6 provides clear information on the preferences of the 20 individuals. The schedule of measuring was conducted in two types, V1 and V2, as described in Table 3.7. Each breath-holding was performed for approximately 30 seconds, and some samples were ignored due to classification ambiguity.

Measurement of a force plate in the form of a bed is used. The force plate had four tensometers embedded in its four corners. Each tensometer could measure the force in three orthogonal directions with a precision of up to 0.1 N. Therefore, it is feasible to obtain 12 force signals. The ECG signal is measured simultaneously with the force measurement. All the signals are registered using a 24-bit AD converter with a sampling rate of 1 kHz. The data are then stored on a computer's hard drive. This yielded 13 time-series, with 12 force signal time-series representing a coordinate projection of a 12-dimensional curve parameterized by time, as shown in Figure 3.6 with an example of three signals.

Data annotation is made manually based on measuring observation. Every measure is represented by a matrix, where rows are individual samples every 1 millisecond and 14 columns are one value of data loading (0 correct, 1 incorrect), twelve force signals, and ECG value. Unlike the other databases, feature extraction is done by the Cartan Curvature method shown in Figure 3.7, where at 300 ms, R peak trigger is shown and from 450 ms to 800 ms is a range of important patterns.

The most important events in a typical cardiac cycle, as described in [16], occur between approximately 150 and 500,ms after the R-peak. The aortic valve opens at approximately 80 ms, and closes at approximately 300 ms after the R peak. The pulse wave velocity through the aorta is approximately 30 m/s. The important reflections of the pulse wave emerge at the aortic arch (in the starting part of the aorta, right next to the aortic valve) and at

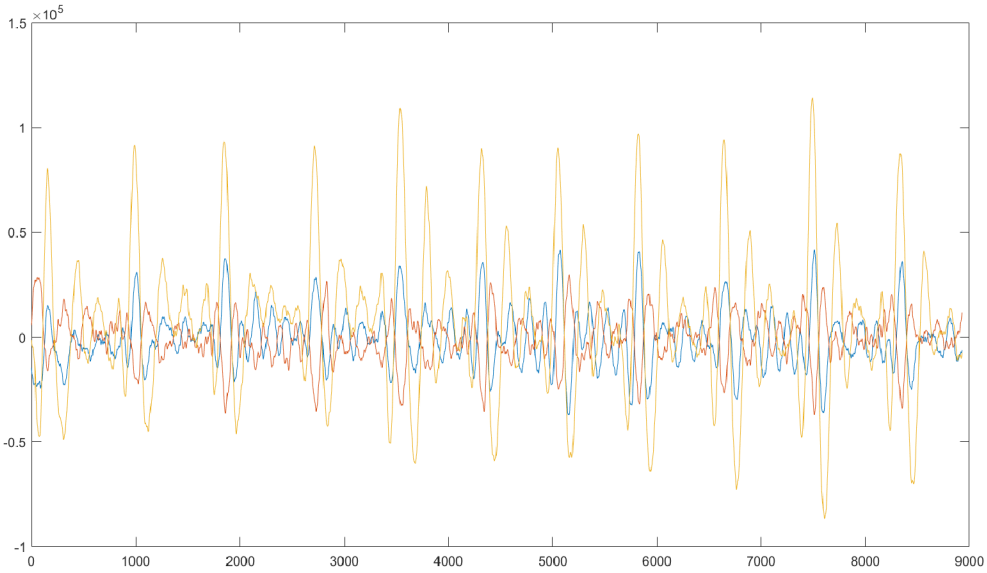

Figure 3.6: BCG experiment measuring [21]

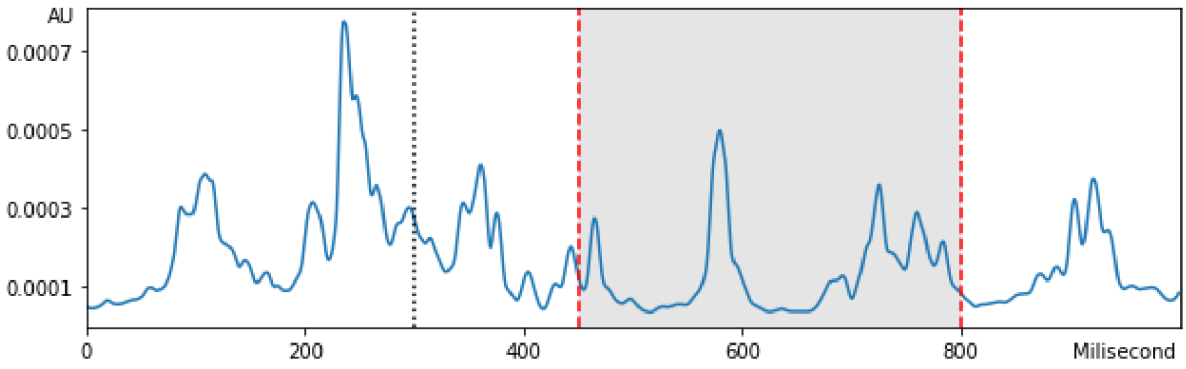

Figure 3.7: Example of Cartan curvature with important section [22]

the bifurcation in the abdomen (ending part of the aorta). The distance from the aortic valve to the bifurcation is approximately 60 cm. This implies that if the pulse propagates immediately after the aortic valve opening, it arrives at the bifurcation in approximately 20 ms. However, the rapid ejection phase of the cardiac cycle takes approximately 100 ms, and thus, the region between 150–500 ms after the R peak is sufficient to record all the important reflections of pulse wave related to changes in blood pressure that is relative to changes in breathing.

3.3.3 Electroencephalography

The first dataset in EEG problematic is the Bonn University EEG database, which was presented by Andrzejak et al. [11], a valuable resource for researchers in the field. The dataset

Table 3.6: List of individuals with their preferences [22]

No. of subject	Sex	Age	Schedule	No. of subject	Sex	Age	Schedule
1	male	26	V1	11	female	62	V1
2	male	26	V2	12	female	35	V2
3	male	23	V1	13	female	65	V1
4	male	28	V2	14	female	35	V2
5	male	28	V2	15	female	35	V2
6	male	28	V1	16	female	35	V2
7	female	24	V1	17	female	28	V1
8	male	30	V1	18	male	30	V2
9	female	36	V1	19	male	33	V2
10	male	30	V2	20	male	33	V2

Table 3.7: Schedules of measuring [22]

V1 schedule		V2 schedule	
Time (s)	Event	Time (s)	Event
0	start of measuring on back	0	start of measuring on back
60	breath-hold during inhalation	60	breath-hold during inhalation
120	breath-hold during inhalation	150	breath-hold during exhalation
180	breath-hold during exhalation	240	breath-hold during inhalation
240	breath-hold during exhalation	330	breath-hold during exhalation
300	legs underlay for position change	420	end of measuring
420	turning on the side		
480	breath-hold during inhalation		
540	breath-hold during inhalation		
600	breath-hold during exhalation		
660	breath-hold during exhalation		
720	end of measuring		

comprises five sub-sets that are divided into three classes based on the type of EEG activity recorded. The first two sub-sets, A and B, contain EEG recordings from five healthy subjects, with the subjects' eyes open and closed, respectively. These recordings provide a baseline for normal EEG activity. The third and fourth sub-sets, C and D, contain EEG recordings from patients with pre-ictal activity, i.e., EEG changes preceding a seizure. These recordings are useful for identifying early warning signs of seizures. The fifth and final sub-set, E, comprises EEG records of a patient's seizure activity (ictal). This sub-set is particularly valuable for studying the characteristics of seizures and for developing algorithms to detect and predict seizures. All the data in the Bonn University EEG database was acquired as 23.6-second samples with a sampling rate of 173.61 Hz. Each sample contains 4097 points, providing high-resolution data for analysis

The CHB-MIT Scalp EEG database, which is the second publicly available dataset, was collected at the Children's Hospital Boston [36]. The dataset consists of recordings obtained from 22 subjects over an extended period of time, including both seizure and non-seizure segments. Unlike the Bonn dataset, which consists of 1-dimensional vectors, the CHB-MIT dataset contains records with 18 to 23 channels and a 256 Hz sampling rate. A channel example is defined in Figure 3.8, with a marking of the seizure part. The dataset is an essential resource for researchers and practitioners who aim to study epilepsy and seizures. It provides a comprehensive view of EEG signals recorded from multiple channels, allowing for detailed analysis and interpretation of the data. The availability of this dataset has greatly facilitated research efforts in the field of epilepsy, and its continued use and development are expected to yield further insights into the nature of this condition.

As a result of prolonged monitoring, the ictal and interictal segments exhibit a marked imbalance, with seizures accounting for less than 2% of the total duration. In an effort to address this issue, the researchers drew inspiration from the work of Wang et al. [92] and proposed a method of balancing the data. To accomplish this, they employed a technique that involved the use of 2-second sliding windows with a 1-second overlap for each ictal record. However, since not every interictal sample could be used from the records, a random selection process was employed to match the number of ictal samples. This allowed for a more balanced dataset and improved the Acc of the analysis.

Expanding on this, it can be said that achieving a balanced dataset is crucial for the accurate analysis of data, particularly in the field of epilepsy research. The proposed approach not only provides a means of balancing the data but also allows for a more efficient and effective analysis of the recorded data. By utilizing 2-second sliding windows with 1-second overlap, the research was able to better capture the relevant information within the ictal segments. This, in turn, allowed for a more detailed and accurate analysis of the data. Furthermore, the use of random selection in the interictal segments ensures that the resulting dataset is representative of the overall data, and minimizes the risk of bias.

3.4 Data processing

The first step in all classification systems is data analysis and preparation. This process is essential in providing accurate data processing which leads to improved performance

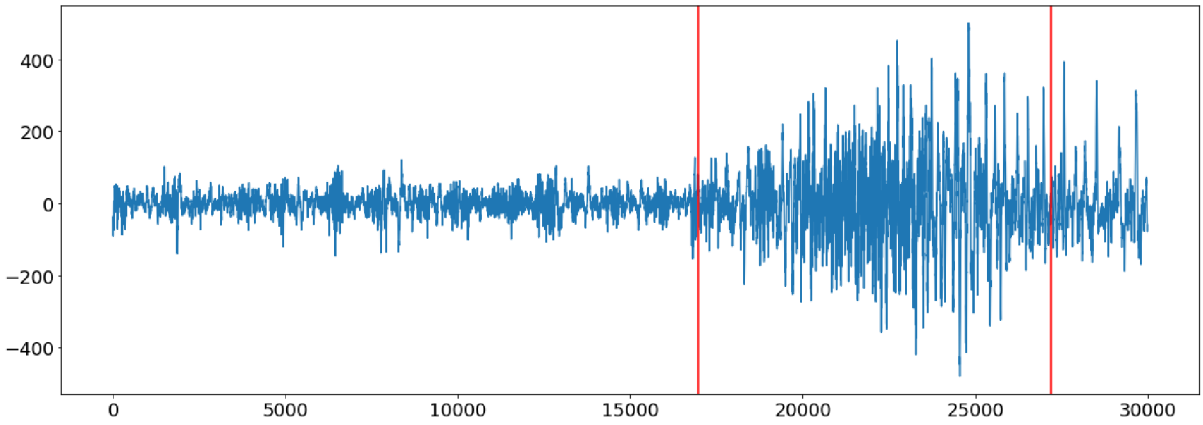

Figure 3.8: Example of EEG with seizure annotation [24]

quality. In this context, the research of data processing was executed on ECG signals to classify heart disease and was published in [32, 33]. To achieve reliable results, it is necessary to understand the characteristics of the input data, including the possible sources of noise and how to preprocess it. Therefore, the chapter begins with a description of potential health problems related to ECG data. This information will provide a better understanding of the importance of accurate data processing in the diagnosis of heart disease.

The clinical diagnosis of arrhythmias includes short-term or long-term measuring of heart operation, which is mainly done by ECG device. The ECG works on the principle of measuring the projection of the heart polarization vector [79]. It is measured by electrodes placed on the human body in the correct position depending on the number of electrodes. It is possible to use only two electrodes but three electrodes have a better signal-to-noise ratio. Additionally, more than three electrodes are used for the measurement of different projections of that polarization vector [95]. The ECG device is a non-invasive tool that measures the electrical activity of the heart, which provides valuable information about the heart's condition. However, the raw signal may contain noise and artifacts that affect the Acc of the diagnosis. Therefore, signal preprocessing is an essential step in the data analysis and preparation phase.

For visual detection options of these patterns, it needs to have a signal-transforming process from electrodes to the output monitor. However, data can be distorted by noise during their transmission which can lead to loss of necessary information. Moreover, due to the connection between A_{fib} and A_{fl}, the similarity of some symptoms, unexpected artifacts, or just faint manifestation of syndromes, can be difficult to recognize each rhythm type or overlook some important sections. An automated CAD is a feasible technique for eliminating

human factors or distorted signals.

To ensure the Acc of the diagnosis, it is crucial to analyze the input data thoroughly. A literature review and analysis of possible improvements in data processing tasks are necessary. The purpose of a literature review is to identify the strengths and weaknesses of previous studies related to ECG signal processing. This information helps to identify research gaps and potential areas for improvement.

CAD systems are commonly implemented using traditional flowchart approaches, which involve several tasks such as preprocessing, feature extraction, feature selection, and classification [39]. These tasks are performed to analyze ECG signals in order to detect various cardiac abnormalities. Preprocessing methods like empirical mode decomposition (EMD) [8], discrete wavelet transform (DWT) [69], Daubechies-6 [4, 6], Z-score normalization [5, 6], and others are commonly used to prepare the ECG signals for feature extraction. For instance, EMD and DWT, can be used in combination with continuous wavelet transform (CWT) [50] or wavelet packet decomposition [19] to extract features based on time-frequency. Furthermore, nonlinear features like recurrence quantification analysis (RQA) can also be used for feature extraction [26].

In the feature selection task, statistical methods such as the chi-square test [55], analysis of variance (ANOVA) [3], Fisher score [28], and so on are frequently employed. These methods are used to select relevant features from the extracted features for further analysis. In the classification task, different techniques such as decision tree [3, 26], support vector machine (SVM) [40, 87], k-nearest neighbor (KNN) [3, 62], neural network (NN) [63, 68] etc., are used to predict the ECG signals into different classes. However, completing all of these tasks can be time-consuming and complex, requiring extensive expert knowledge of internal functionality.

Acharya et al. [3, 5, 6], developed various CAD systems for detecting heart diseases from ECG signals. In their first work [3], the researchers focused on the characterization of arrhythmias using nonlinear features. They proposed a system that employs thirteen different types of nonlinear features that are ranked by ANOVA and classified with the KNN and decision tree (DT) classifiers. The innovation of this paper, compared to previous works, is that the new approach includes only simple standardization with classifiers, so preprocessing and feature extraction are not necessary to compute before arrhythmia recognition. This provides a more practical innovation for CAD.

Nevertheless, they employed some techniques that do not require strict adherence to standardized procedures. In the following paper [6], the researchers presented an automated detection system for arrhythmias using a CNN. All ECG signals are preprocessed with Daubechies wavelet 6 and classified into two different architectures based on segment intervals. This approach achieved an Acc of 98.52%, a Sen of 98.02%, and a Spec of 99.01%.

Furthermore, Acharya et al. developed a different CNN model for identifying shockable and non-shockable life-threatening ventricular arrhythmias [5]. They preprocessed ECG segments in the same manner as in the previous article, which yielded Acc, Sen, and Spec of 93.18%, 95.32%, and 91.04%, respectively. This paper provides evidence of the effectiveness of using CNN for detecting life-threatening ventricular arrhythmias, where the CNN eliminates feature extraction separately and learns the features directly from the input data, making it easier and faster to analyze the input [54]. These articles, on the other hand, employ Z-score normalization, computed by mean and standard deviation. These parameters must be calculated from the dataset, implying that the CNN model depends on the data used.

Prior to classification by CNN, CWT was used in the first research [33] to divide ECG signals into wavelets by:

$$CWT(t) = \min\left(0.1, \Psi^2_{T,s}(t)\right), \tag{3.1}$$

where Ψ denotes a Morse wavelet with a time bandwidth of T and symmetry s in the extracting sample's time t. Following a closer examination of the extraction results, T was set to value one and s to value 2. The choice of T and s values is crucial for obtaining a good feature extraction output. These values determine the wavelet's scale and frequency, respectively, and they need to be chosen carefully based on the properties of the analyzed image. Besides that, every parameter after CWT with a greater value than 0.1 was set on itself for optimal extraction of necessary features. The power of two was used to ensure only positive numbers and easier conversion to a range of 0-255, representing the image's colour components.

To visually represent our feature extraction process, grayscale versions of the extracted features for each class are shown in Figure 3.9. These examples serve to illustrate the effectiveness of the extraction method and demonstrate the distinct features that are captured for each class. By carefully selecting and fine-tuning our extraction parameters, the system ensured that the extracted features were informative and accurate, which is essential for

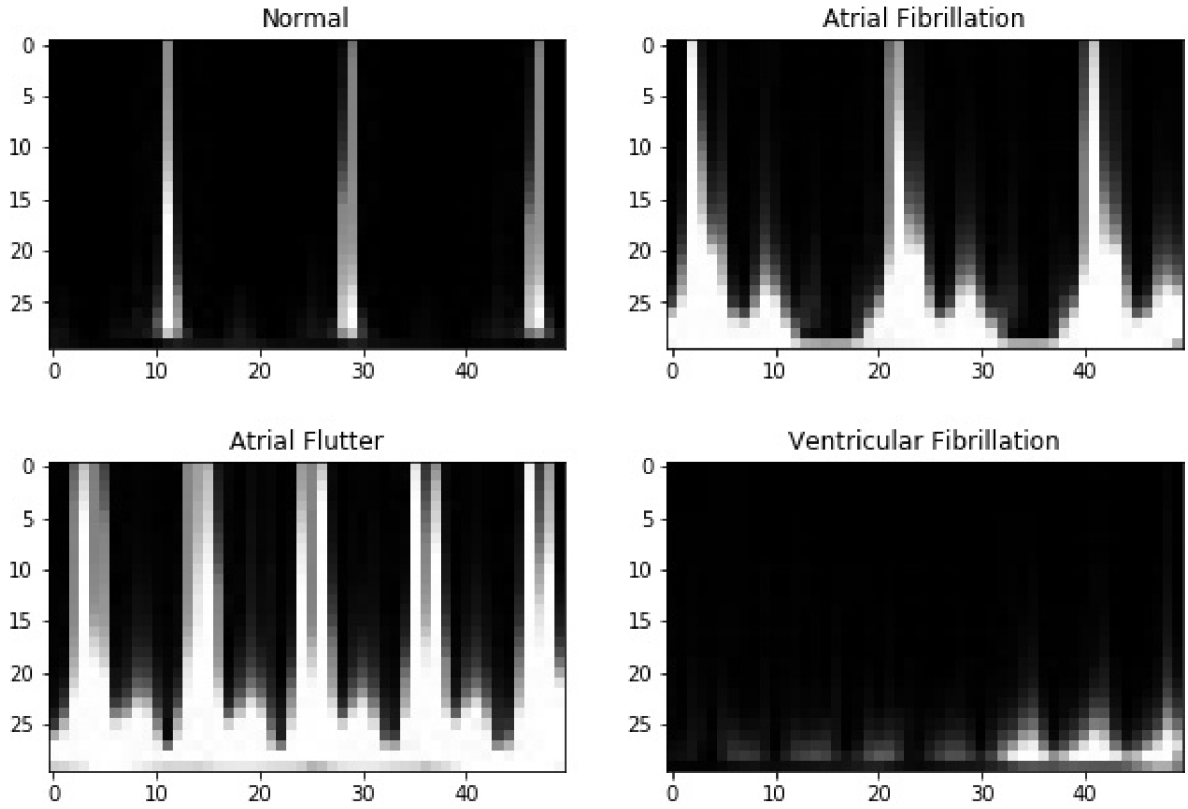

Figure 3.9: An illustration of CWT of normal, A_{fib}, A_{fl}, and V_{fib} patterns [33]

further analysis or modeling work.

In contrast with traditional machine learning techniques, this study presented a 6-layer deep CNN model to 4 classes (normal, A_{fib}, A_{fl} and V_{fib}) recognition of ECG rhythms. The proposed model needs no user interference and R-peak detection is not required. Also, three MIT-BIH PhysioBank databases were used to train and test the CNN model. CNN model can be implemented in the healthcare industries as an added tool to assist physicians in providing a decision support system on the diagnosis. The presented model can also be used in the home environment for watching elderly patients by their family members for analysis of heart problems.

In these approaches, where some of the processes from traditional system flowcharts are omitted, there is very important to consider some validation threats. From an external perspective, it is necessary to normalize inputs into the same form. Typical normalization of data is to watch on a different frequency of measuring. If the data are not normalized, it can happen that input into the system contains shortage or surplus information, and the classification process is not valid. Another problematic part is that our approach works with lead II ECG signals from 12 possible leads for measuring. Every single lead could have a

different projection on the polarization vector, including different views on heart activity. In this way, using more than one lead can cause a malfunction of prediction. Internal perspective comprises operation on data before classification itself. Ignorance of input and use of preprocessing or feature extraction methods can lead to loss of important information on the account right classification. Another important aspect is the design of neural network architecture. Often the problem is a too-robust solution where a network includes more neurons than is needed for sufficient functionality. At first sight, it may seem like the problem of computational complexity only, but actually, it can lead to the dysfunction of the whole system. If the network contains too many neurons, many inputs can be classified by a single branch regardless of others; in such a context, clarification can provide great Acc, but the prediction on the total new dataset could have insufficient results.

Since two of the databases are sampled at a frequency of 250Hz, and the last one is sampled at a frequency of 360Hz, the length of the input vector to CWT was used as 500 and 720, respectively, representing an ECG signal with a 2-second duration. Output 2-dimensional matrix was resized to a width and height of 50 and 30 pixels, respectively, which guarantees optimal input to CNN without previous up-sampling, down-sampling, or normalization of the signal.

For a summary of the methods used for data processing, some articles are based on R-peak detection [3, 26, 40, 63, 71, 101]. However, needs long segments for a finding of the R-peak or QRS complex which makes it not possible to real-time classification. Above that, denoising methods are used for smoothing the signal [3, 5, 26, 40, 63, 98]. There are approaches where noise can have a big impact on the final system result. In the case of CNN, raw data can have worse Acc, but still within acceptable limits, and sometimes, if data are different, the model's performance can be almost the same. The next problematic issue is separate feature extraction, feature ranking, and classification [3, 26, 40, 63, 71, 78, 101], which require knowledge of all different algorithm for the right use. Acharya et al. [5] and Xia et al. [98] is most close to this paper. Nevertheless, Z-score normalization depends on knowledge of all datasets to compute the mean and standard deviation. In the second case, wavelets are useful, like feature extractors too, so in combination with CNN are redundant, network input has higher resolution, and the CNN model must be more complex with more neurons.

For that reason, there is a need for preprocessing that depends on knowledge of data

characterization for each class, not on the dataset or several different methods. The objective is to show the robustness of CNN architecture, which can replace some processes of traditional CAD system flowcharts. It could reduce the computational complexity of arrhythmia detection and dependency on using the dataset. This could provide a useful easy implementation for the practical medical environment for real-time decision support.

3.5 Data fusion

The next step in designing the system is fusion in cases where more channels are measured, unlike the case of ECG. Fusion can occur in two scenarios, namely during multi-channel measurement or unification of time series when the trigger is known (e.g. heartbeat). The first type, represented by EEG, involves measuring multiple channels simultaneously. In this case, fusion occurs when data from each channel are combined into a single output signal. The second type, represented by BCG, involves measuring data over time. In this case, fusion occurs by unifying the time series into a single output signal.

3.5.1 EEG

In the case of EEG, classification should be performed on one-dimensional vector inputs. Anyway, some systems must process more signals to arrive at a result. The first type of system deals with a combination of different types of data like ECG and photoplethysmogram (PPG), which can be used for blood pressure prediction [35] or heart rate variability [47]. On the other hand, some devices provide the multi-dimensional output of the measuring process like EEG for epilepsy detection, which experiments were published in [24].

Classification models of EEG could take the form of conventional statistical approaches like KNN [13, 29], random forest (RF) [93], linear discriminant analysis (LDA) [91], or SVM [56, 104]. Li et al. [57] proposed a method based on channel selection by computing the standard deviation for each and nonlinear mode decomposition for three different classifiers: SVM, KNN, and LDA. The KNN model achieved the best performance of tested parameters of Acc, Sen, and Spec. Another study by Anuragi et al. [12] introduced a novel algorithm that obtains features from euclidean distances of sub-bands phase-space representation and Fourier–Bessel series expansion from empirical wavelet transform. Seven different classifiers have been tested with the optimal number of features selection. Amiri et al. [10] presented

a process based on feature extraction from the time-frequency planes of optimal channels. Their channel selection strategy does not disregard channel correlation due to a sparse common spatial pattern. Compared to Perceptron and Linear SVM, LDA outperforms the other two tested classifiers.

The literature contains several approaches based on one EEG channel with the deep learning process from base neural networks to their modifications like recurrent neural network (RNN), or CNN. For instance, Qaisar et al. [72] proposed an effective method based on one EEG channel and neural network. Zhang et al. [105] employed RNN, while Wei et al. [94] used CNN for the same purpose.

Sadiq et al. [77] exploited ten well-known pre-trained CNN models on CWT images. Meanwhile, Mandhouj et al. [60] extracted features by short-time Fourier transform (STFT) instead and designed a 2D CNN architecture to recognize ictal, inter-ictal, and health classes. Nevertheless, several types of research proved no need for feature extraction. Acharya et al. [7] presented the first deep neural network application for EEG-based seizure detection. They preprocessed the data by performing Z-score normalization, zero mean, and standard deviation, followed by a 13-layer deep one-dimensional convolutional neural network.

However, EEG classification is not provided only on the one-dimensional vector [14]. Some studies have employed a multi-channel dataset and different strategies for dealing with one-dimensional CNN. Wang et al. [92] linked all channels in series, rather than in parallel, to convert input from two-dimensional to one-dimensional. Gao et al. [34] invented generative adversarial network (GAN) and CNN architecture based on each channel classification separately. Post-processing channel fusion with the threshold for judging seizure and non-seizure records resulted in the final classification.

The current solutions for CAD have some flaws in their deployment that need to be addressed. One major issue is the channel selection in cases of multi-level measuring, which has been discussed in a recent study by Amiri [10]. In real-time applications, selecting based on knowledge of the entire dataset is impossible. Problem detection has to be performed on actual data without any prior knowledge. Assuming all available information is used, it may be problematic if the measuring does not follow the same channel strategy. This could lead to an unstable input format, resulting in different architectures for every measurable difference.

Another disadvantage of current CAD solutions is the complexity of the solutions them-

selves. In previous research works, the data was preprocessed for smoothing and extracting features. However, in the case of multi-channel measuring, redundant information is included, which extends calculation time beyond the system's needs. Therefore, this research aims to simplify the input while maintaining information integrity to find the ideal CNN architecture. The research draws inspiration from well-known multidimensional transfer learning solutions.

3.5.2 BCG

Breathing disorders cannot be detected as easily as fibrillations or seizures because their detection requires longer-term measurements. Unlike fibrillations or seizures, which can be detected in short segments, breathing disorders often require monitoring over a period of time to diagnose and treat accurately. In [107], a novel approach is proposed for detecting a long-term heartbeat cycle length. They measured both BCG and ECG concurrently to assess the correlation between the beat-to-beat cycle of both types of sensors. The results showed that the correlation of the cycle length was 0.95 with an absolute difference in the cycle length of 4 ± 72 ms. A piezoelectric foil sensor was used, and persons were examined in a lying position on the back because it is necessary for achieving good results.

In [100], they proposed an algorithm for separating the cardiac and respiratory components with noise reduction on the heart rate and respiration components of BCG signals. It was done by the locally projective noise reduction algorithm for denoising deterministic chaotic time series. It can be applied to signals which are not cleanly deterministic, like physiological time series like ECG, BCG, and EEG.

In another article [45], Hwang et al. collected overnight polysomnography and ballistocardiography recording pairs from patients with and without nocturnal hypoxemia. By the regression analysis, they achieved an average Acc of 96.5%. Sadek et al. [76] evaluated the capacity of the micro-bend fiber optic sensor to monitor heart rate and respiration in a non-intrusive manner. In addition, they tested the discrimination between shallow and no breathing. Their approach highly correlated the heart and breathing rates, 0.96 and 0.78. However, the proposed sensor provided a very low Sen of $24.2 \pm 12.81\%$ and Spec of $85.88 \pm 6.01\%$.

Liu et al. [59] studied the detection of obstructive sleep apnea. Their algorithm first preprocesses the raw BCG data and locates potential event segments by detecting arousals.

Thereafter, the distribution of each potential event into three phases and the selection of features to detect respiratory patterns were done. They then used a backpropagation neural network to classify these events into apnea and non-apnea classes. The experimental results based on a real BCG data sheet revealed that the Acc, recall, and area under curve (AUC) were 94.6%, 93.1%, and 95.1%, respectively.

Zink et al. [107] used the BCG signals to detect variations in the heart rate associated with sleep apnea syndrome. The authors applied wavelet decompositions extraction to analyze the BCG signal and obtain the heartbeat interval. These features were used as input to a support vector machine classification model. Experimental results on 42 subjects with 5-fold cross-validation achieved a 90.46% precision rate and 88.89% recall rate. In the last relative article [88], the signals of five sensors and their placement combinations for measuring a sleeping person were compared from the perspective of their measurement sensitivities and waveform quality. In conclusion of this paper, the heartbeat and respiration parts are represented the best in the signals measured with the mattress force sensors.

In our first BCG research [21], we presented a novel approach for recognizing the form of breathing independent of the body position by BCG sensors. The signals were processed by Cartan curvature and extracted pulse arrival time related to human respiration and blood pressure via the Moens-Korteweg relation [70]. Thereafter, the breathing anomalies were detected between heartbeats measured by ECG and the pulse arrival times, as shown in Figure 3.10. These delays were used as the inputs to CWT for parameters and power analysis before training a CNN classifier.

One of the main differences between the work and other articles is that our approach is independent of the position of the sensors on the measuring bed. Using Cartan curvatures and the Moens-Korteweg relation, it is possible to determine various physiological dependencies with notable signal-to-noise ratios. However, the system required significant preprocessing before applying the CNN architecture, unnecessarily increasing the computation time for recognizing breathing disorders. The differences in delays between individual heartbeats are also in milliseconds, making the model very sensitive. As a result, we experienced problems correctly detecting breathing in individuals lying on their sides.

In the next paper [22], we introduce a novel approach to process and classify ballistocardiography signals for detecting breathing disorders. Our method uses optimal formulas of Cartan curvatures to recognize breathing problems, regardless of body position during

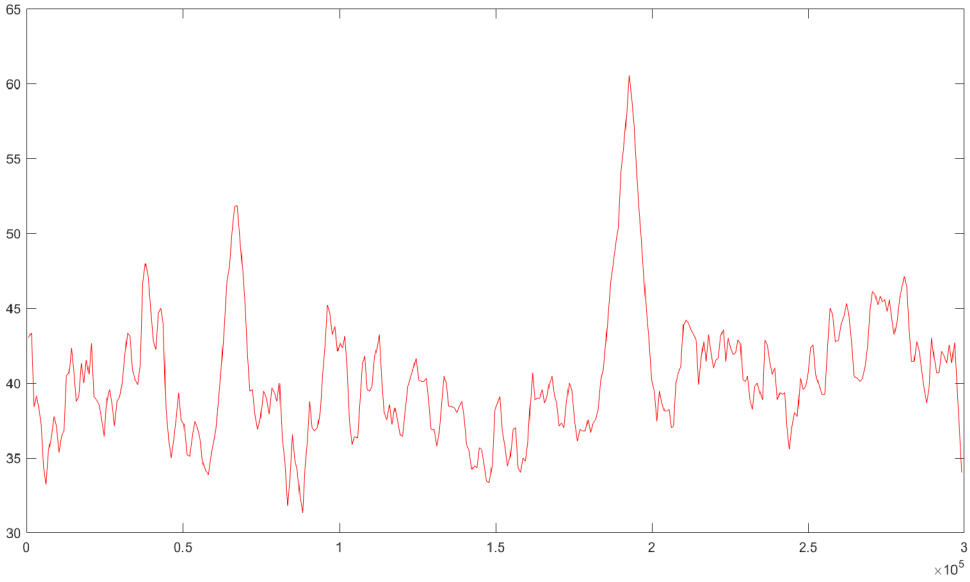

Figure 3.10: Pulse wave times (x: time/ms, y: pulse arrival time minus constant) [21]

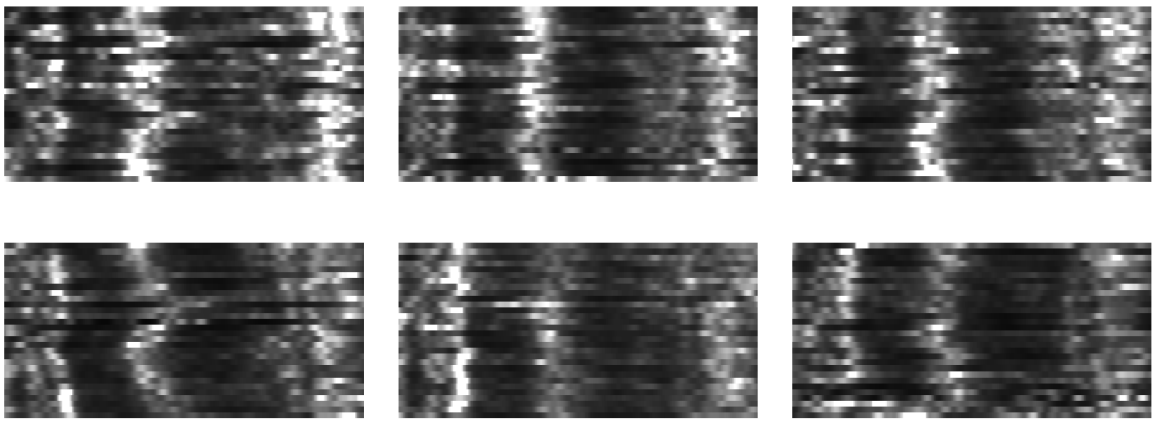

Figure 3.11: Examples of classifier input (Top: regular breathing; Bottom: disorder breathing) [22]

measurement, and with greater clarity than our previous work. We begin the paper by presenting the classical method for R peak detection from the electrocardiogram ECG signal. Then it continues with a formulation of Cartan curvatures and a description of information, which can be found in. The last part of data processing is preparing the input for the CNN classifier. Data are converted to a grayscale image and resized to 30 x 150 for optimal input in case of algorithm asymptotic complexity. Several examples of network input are shown in Figure 3.11, where regular breathing is placed at the top and disorders at the bottom.

In our recent paper [23], we propose a novel approach to detecting breathing disorders using a mechanical trigger based solely on BCG data. Using the BCG data enables the

system to be truly unobtrusive. Our trigger is based on detecting the ejection of blood from the heart, and we leverage differential geometry invariants to propose a new differential invariant, the Euclidean arc length [96]. This invariant can serve as a trigger for categorizing Cartan curvatures in CNN. One of the major advantages of our mechanical trigger is its complete unobtrusiveness. Additionally, the properties of our trigger are invariant in the same way as Cartan curvatures, allowing for its applicability for individuals lying in different positions on a bed. Furthermore, the arc length is calculated directly from the measured signals, simplifying the process.

In summary, our previous work [21, 22] was founded on three fundamental pillars: identifying triggers for individual heartbeats, calculation of Cartan curvatures, and the processing of results using CNN. In this paper, we introduce a new algorithm to calculate the first part, the trigger, which must be highly precise to capture subtle variations in pulse arrival time that are then processed using Cartan curvatures. The primary novelty of this paper is also the implementation of this new trigger and the improvement of the CNN to develop a completely unobtrusive mechanical system without the need to connect any equipment to the measured person or use any ionizing radiation for measurement, unlike similar systems presented in the literature. The typical shape of the monitoring function is shown in Figure 3.12.

Our previous work established the foundation for our current research, where we sought to address a critical issue in monitoring the health of individuals. Accurate monitoring of pulse and heartbeats is essential for detecting and diagnosing various cardiovascular diseases. However, existing methods for monitoring heartbeats require connecting various equipment to the individual being monitored, which can be invasive and uncomfortable.

The QRS complex and the T wave provide valuable information for distinguishing separate parts of the signal. With this in mind, we have decided to use the maxima of a monitoring function as the trigger for our preprocessing sequence. This maximum corresponds with the end of the rapid ejection phase, which then translates into a reduced ejection.

It is worth noting that the distance between the mechanical trigger and the R wave varies over time and depends on various physiological phenomena and thoracic pressure. On average, however, the distance is 160 ms $\pm$ 40 ms. This variability in the distance emphasizes the importance of selecting an appropriate trigger for our preprocessing sequence, as it ensures that the signal is properly segmented and analyzed.

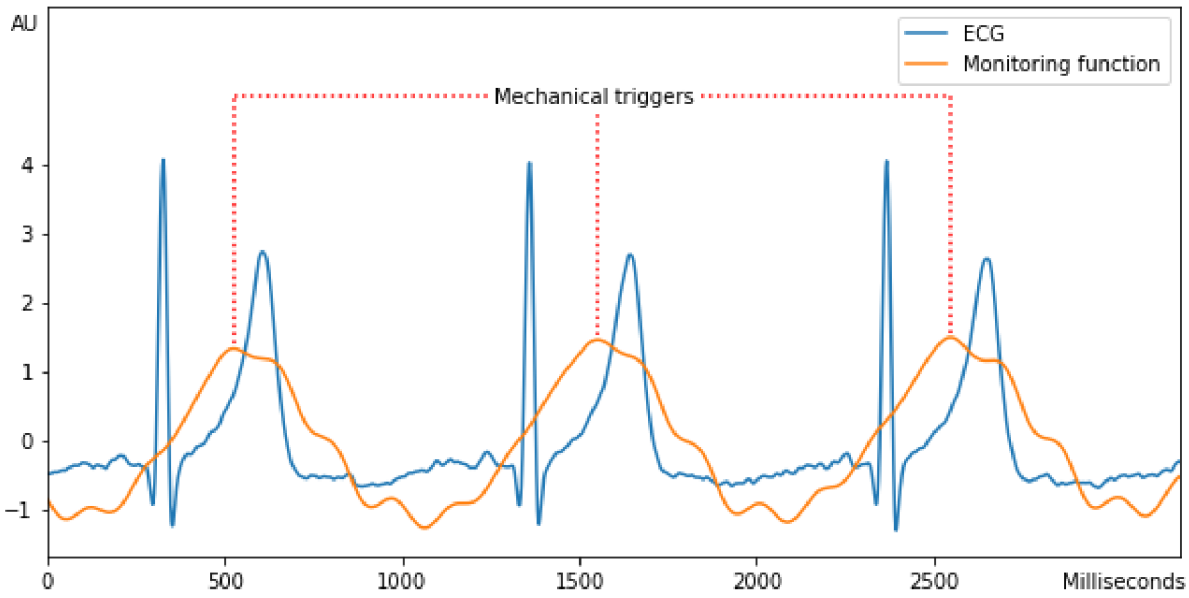

Figure 3.12: Ilustration of ECG and Euclidean arc length [23]

As each sub-investigation had its timeline, data fusion for EEG was performed at a later stage. As a result, in all related works, the input to the CNN was two-dimensional. However, subsequent experiments revealed the effectiveness of data fusion, and a back-analysis was also conducted for BCG.

3.6 CNN

Once data has been appropriately processed, it becomes crucial to verify the effectiveness of the classifier and the complexity of its internal parameters, which together make up the resulting architecture. To optimize the performance of CNN models, several options exist for reducing computational complexity without sacrificing Acc.

3.6.1 Model reusability

Recently, classification in clinical behaviors is performed by deep learning techniques. These techniques have proven to be effective in improving the Acc of image [81], text succession [51], and speech recognition [1]. They consist of several types of layers that are designed for pattern searching and classification. Since the input image is represented by 2D or 3D matrices of numbers, CNN can be used on any sequence, even on 1D signals, as presented above.

Regarding image data classification, it is common to use pre-trained architectures instead of creating the original architecture of the neural network. The internal model parameters of pre-trained architectures are already set by previous training, so they are not initialized pseudo-randomly according to the selected optimizer [38]. Following that, these pre-trained models are then tailored to the specific problem at hand. This is achieved by creating a specific dataset divided into classes that must be distinguished and used in a new training process. The advantage of pre-trained models is that they have been trained on millions of internal parameters and tens to hundreds of class types. This makes the hidden layers of these networks well-equipped for specific image recognition problems. However, they may not be suitable for vital sign data classification due to two main factors.

The first factor is that the pre-trained models are designed for image recognition which is not one-dimensional. As described above, converting one-dimensional data into a two-dimensional form through one of the methods of preprocessing or feature extraction did not improve classification Acc. This conversion requires additional computation beyond what is necessary, and the architecture must contain more internal parameters to perform the classification task.

The pre-trained neural network architecture used for image classification has a significant limitation in the dataset used to train its internal parameters. While the neural network is specifically designed for image classification, the input data used for its training doesn't include critical classes such as vital data. This absence of crucial information may limit the network's performance in identifying and addressing critical issues. Therefore, expanding the dataset used to train the neural network to include vital data classes is essential. By incorporating more diverse and critical information into the training dataset, the neural network will be better equipped to identify and address crucial issues accurately and reliably.

In our previous work [23], a limitation was tackled in identifying breathing disorders by employing a specific neural network architecture. The input data was a two-dimensional matrix that comprised 30 consecutive slices of the measured data, each of equal length. The matrix was processed by the neural network to identify and classify different breathing disorders based on the patterns in the data.

The model's results were compared to those of well-known pre-trained architectures that had been fine-tuned for the same research issue with the same hyperparameters settings. These results are shown in Table 3.8. The presented solution achieves comparable

Table 3.8: Comparison with well-known implementation of advanced CNN models [22]

Model	No. of parameters	Acc (%)	Sen (%)	Spec (%)
Current [22]	97,247	96.37	92.46	98.11
ResNet50 [42]	25,636,712	97.03	94.75	98.05
DenseNet121 [44]	8,062,504	96.76	98.69	95.91
MobileNetV2 [43]	3,538,984	95.01	85.15	100
Xception [18]	22,910,480	92.85	91.27	93.57
NASNetMobile [108]	5,326,716	94.88	83.01	95.71

performance. Furthermore, the well-known classifiers we tested are prepared for many image classifications and include millions of trainable parameters. In contrast, our model has fewer than 100,000 trainable parameters. The existing architectures have a much higher level of complexity than our model, which makes them more computationally demanding in subsequent applications. Using an optimized architecture significantly reduces the need for computing power when using the classifier.

Given that existing neural networks for image data classification can be used to classify various image issues, a hypothesis is offered about the reusability of the one-dimensional convolutional neural network architecture for various vital data classification issues. In the case of images, however, the higher complexity is not only in the fact that images have a higher dimensional order than vectors. It is necessary to realize that in most cases, it is a capture of the real-world three-dimensional objects containing, in addition, a different colour component described using different colour channels according to the sensing method. There is a need for input data with the object of interest from different points of view and colours for correct classification, which includes a large variability of individual classes. The second point can be partially replaced by augmentation methods, leading to the expansion of the collected data. In the case of vital data, these complications do not occur, and the only problem is the diversity of data obtained from different individuals with different physiological characteristics. However, this does not change the fact that the given differences in the individual classes (generally healthy data versus data with certain health complications) can be described.

In correlation with a described hypothesis about the reusability of the model, the research of ECG and EEG were tested with the same CNN architecture both separately and together.

3.6.2 Frequency and architecture analysis

Moreover, in the image classification area, pre-trained model input usually does not resolve today's sensing devices. It is due to the need for the low quality of the object in the image. CNN models need to recognize the main patterns that distinguish classes from each other. On the contrary, excessive object resolution leads to redundant information that increases the complexity of the model but does not improve performance. For this knowledge transfer from image to vital data classification, frequency reduction experiments were performed on the EEG dataset to find the point of reduction, which resulted in a lower number of architecture inner parameters without the loss of patterns in signals.

When considering the appropriate frequency for a given issue, evaluating whether the chosen architecture is suitable is crucial. The architectures described in section 3.1 were created using brute-force experiments to reach the optimal amount of layers, filters, and core size. In the framework of previous scientific publications, analyses of the number of filters were made based on individual pieces of training, and adjustments to these numbers were made based on the investigation of the training process and results. Firstly, the initial number of filters was set. In cases where the classification result was insufficient, the number of filters was increased until the classification Acc plateaued. If the classification was sufficient after initialization or if the phenomenon of neural network overfitting was occurring, the number of filters was reduced until this architecture reduction did not affect the classification results.

In the context of training neural networks, the brute-force technique is not a feasible option due to its excessive computational and time requirements. It is impossible to run computations on all possibilities, making it necessary to find other ways to optimize the neural network. The size of the kernel for convolutional layers is determined through data analysis and an understanding of the convolutional operations' purpose. However, this may not always yield the best possible outcome for the neural network.

A fixed number of convolution and max-pooling blocks are used to determine the optimal neural network architecture to examine the input to a set depth. This approach enables the testing of various combinations of the number of blocks, the number of filters on the convolutional layer, and varied input frequencies. Previous experiments evaluated the frequency, but the variable number of blocks allows for different frequency sizes to be employed in the neural network.

Table 3.9: Tested block variations with properties [created by the author]

No. of blocks	blocks kernel size	minimal CNN output
2	19;11	42
3	19;19;11	104
4	19;19;11;11	190
5	19;19;11;11;11	369

Table 3.10: Tested frequencies variations with properties [created by the author]

Data	Frequencies				No. filters
No. blocks	5	4	3	2	
BCG	1000;600;400;369	250;225;200	150;104	42	$\{5 \cdot k \mid k \in [2..12]\}$
ECG/EEG	250;225;200;185	150	100;52	21	

Although the frequency was evaluated in the previous experiment, the variable number of blocks allows for different sizes of frequencies that may be employed in the neural network. Smaller frequencies cannot be processed if the number of blocks is too great since the output of the max-pooling layer cannot be further split. Combinations of a tested number of blocks are specified in table 3.9, with the kernel size of each sequential block and the potential size of input that may be processed by the model. Hyper-parameters like learning rate or optimizer are not changed from the common setting described in section 3.1. Following that, table 3.10 contains information on tested frequencies for distinct blocks. The removal of each block caused the frequency to be tested with a higher frequency. Thus frequencies were tested with further variants and all instances from the preceding experiment. This approach ensured that each frequency range was adequately tested to identify the optimal configuration for the neural network.

4

Results and discussion

4.1 Data processing

The methodology presented in the following section is based on the knowledge of data patterns for each class, without depending on the dataset or pre-processing methods. The objective is to demonstrate the robustness of the CNN architecture, which has the potential to replace some of the processes of traditional CAD system flowcharts. By doing so, the computational complexity of arrhythmia detection could be reduced, and the dependency on the dataset could be minimized. A useful and easy-to-implement solution for the practical medical environment could be provided through the implementation of this methodology, offering real-time decision support to clinicians. The CNN architecture's ability to recognize patterns in data could significantly reduce the need for manual intervention in the diagnosis process, improving the speed and Acc of arrhythmia detection.

4.1.1 Normalization

To normalize the data, we implemented a simple formula that can alter the range of measured samples without requiring high computational complexity and without compromising essential information for future classification. The formula has the form

$$p_i = \frac{\max(-1, \min(1, o_{i+1} - o_i)) + 1}{2}, \tag{4.1}$$

where p_i is i-th value of normalized sample computed from raw samples o on the positions of i and $i+1$. Because the QRS complex can have a different form and value ranges for each person, all numbers less than -1 are set on it and all numbers greater than 1 are set

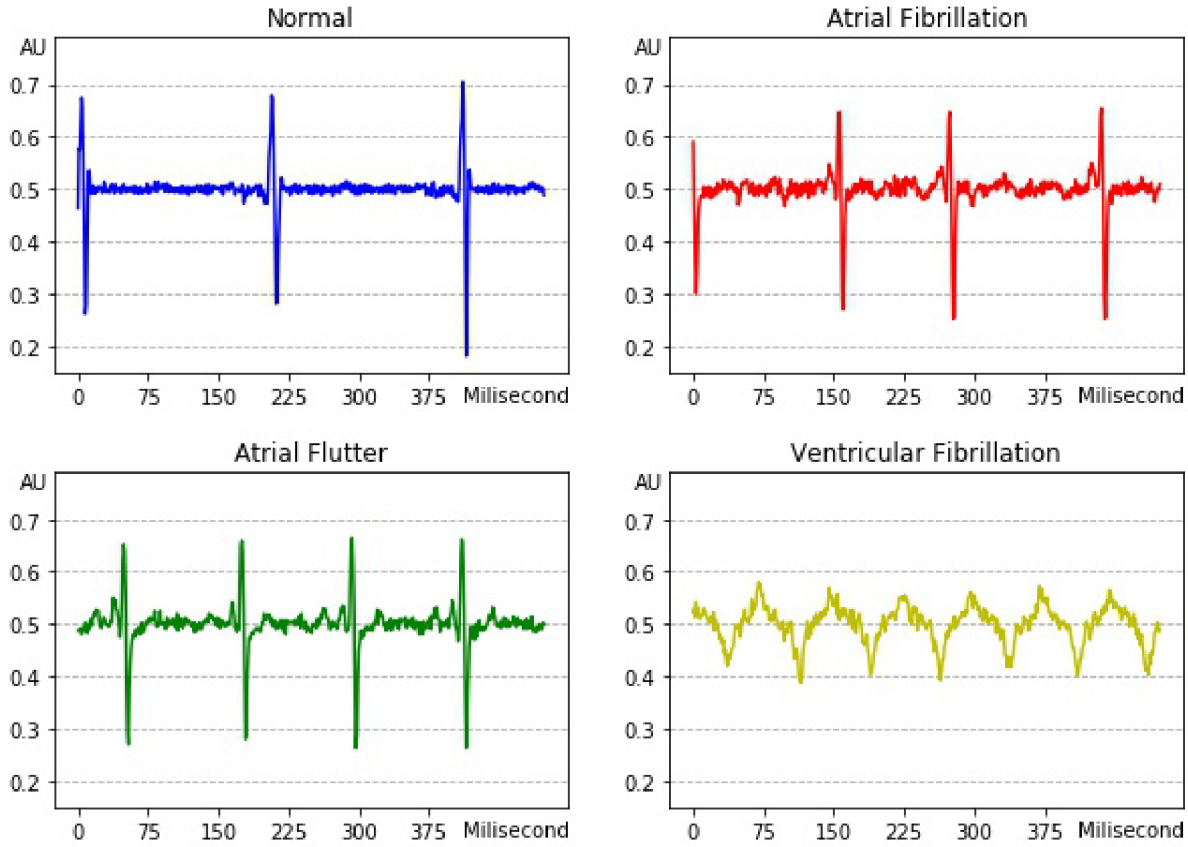

Figure 4.1: An illustration of ECG segments of normal, A_{fib}, A_{fl}, and V_{fib} patterns after normalization [32]

on 1. Thanks to the shapes and properties of ECG signals in general, it is possible to use this elementary operation. The CNN model requires information about the pattern of the P wave and the only positions of the QRS complex, not its power. Due to the main concept of CNN functionality, especially convolutional layers, the range of input data is changed from $(-1,1)$ to $(0,1)$. In this way, it is not necessary to provide R-peak detection or some types of preprocessing methods. Sample examples of all four categories of normalization are shown in Figure 4.1.

4.1.2 Results

The first experiment focused on evaluating the performance of the proposed CNN model in the area of detecting all classes. The results of this experiment are shown in Table 4.1. The table reveals that the proposed model was able to classify 99.79% of the samples correctly as normal. However, the Sen of A_{fl} was found to be less than 90%, with 13.08% of A_{fl} category being wrongly classified as part of the other categories. Among these, 89.59% were bad

Table 4.1: ECG confusion matrix [32]

O/P	Normal	A_{fib}	A_{fl}	V_{fib}	Acc (%)	PPV (%)	Sen (%)	Spec (%)
Normal	3539	11	8	9	99.79	99.27	99.21	99.88
A_{fib}	11	19164	76	21	98.61	98.74	99.43	96.07
A_{fl}	13	198	1469	10	98.80	94.59	86.92	99.64
V_{fib}	2	35	0	929	99.69	95.82	96.17	99.83

Table 4.2: ECG overall classification [32]

O/P	Normal	Arrhythmia	Acc (%)	PPV (%)	Sen (%)	Spec (%)
Normal	3539	28	98.45	99.88	99.87	99.27
Arrhythmia	26	21902	98.45	99.21	99.27	99.87

predictions like A_{fib}. A similar pattern was observed in A_{fib}, where 70.37% of the wrongly evaluated inputs were classified as A_{fl}. This indicates a possible relationship between these classes.

To better understand the performance of the proposed model in distinguishing normal rhythm from arrhythmia, Table 4.2 was generated. This table shows that the normal category has the same value as that in Table 4.1. Normal category predicted as Arrhythmia refers to the summarization of normal samples predicted as A_{fib}, A_{fl}, or V_{fib}. The Arrhythmia category evaluated as Normal is a summary of A_{fib}, A_{fl}, and V_{fib} evaluated as normal. The correctly detected arrhythmia is the rest of the table. Overall, the proposed model achieved an average Acc of 98.45%. Furthermore, Sen and Spec of 99.87% and 99.27% were respectively computed for the normal class. PPV was obtained as 99.88% for normal rhythm and 99.21% for the remaining classes of the proposed model.

The second experiment focuses on the computation time required for the normalization and classification of input signals in real-time, such as a stream from an ECG device. To accomplish this, a simulation of several devices was created using program threads for parallel processing [9]. These simulated devices used the same CNN model for evaluation on a single processor. The system was then tested on a 10-second sample measured with a frequency of 250Hz and 360Hz, with the downsampling of input realized in the latter case. The evaluation was performed with a change of 5 values, which guaranteed the feasibility of 50 predictions per second. Figure 4.2 illustrates the average time required for 10 iterations of calculations and classifications. It is evident that, after including the ECG data transmission time, using one server to manage multiple devices is acceptable in this scenario. The

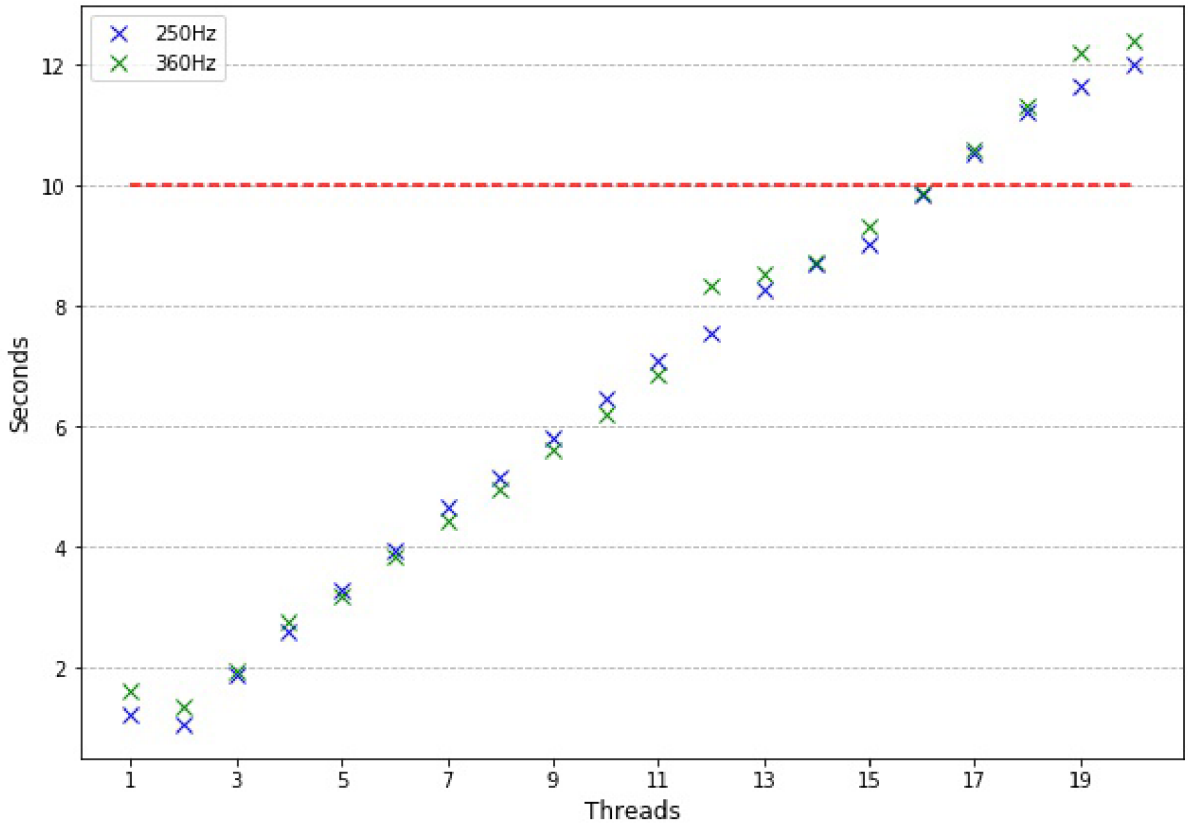

Figure 4.2: Time needed to signal processing and classification [32]

implementation of multiple devices as program threads for parallel processing, using the same CNN model for evaluation, shows as a promising approach for achieving real-time classification of input signals.

Moreover, the tabulated confusion matrix for recognition of normal, preictal, and seizure classes from one-channel Bonn University EEG database is presented in Table 4.3. Preictal and seizure classes were summarized as a representation of abnormal data in order to calculate Sen and Spec correctly. Small differences and values greater than 90% indicate that the classification is balanced and not overfitted. Moreover, the voting method across CNN inputs from single segments was made for proper comparison with other research. It leads to Acc, Spec, and Sen improvements of 98%, 98.5%, and 98%, described in Table 4.4 by the confusion matrix and Table 4.5 with an overall classification of normal and abnormal cases. It is clear that post-processing is required to eliminate potential false detections that could result in a false alarm or overlooking a problem.

Table 4.3: Confusion matrix of Bonn dataset [24]

O/P	Normal	Preictal	Seizure	Acc (%)	PPV (%)	Sen (%)	Spec (%)
Normal	748	34	18	96.37	95.60	92.46	98.11
Preictal	8	759	33	96.37	96.70	98.11	92.46
Seizure	23	15	762	96.37	96.70	98.11	92.46

Table 4.4: Confusion matrix of Bonn dataset after voting method [24]

O/P	Normal	Preictal	Seizure	Acc (%)	PPV (%)	Sen (%)	Spec (%)
Normal	98	1	1	98.33	97.03	98	98.5
Preictal	2	97	1	98.67	98.97	97	99.5
Seizure	1	0	99	99.33	98.02	99	99

Table 4.5: Overall classification of Bonn dataset [24]

O/P	Normal	Seizures	Acc (%)	PPV (%)	Sen (%)	Spec (%)
Normal	197	2	98.33	98.69	98.5	98
Seizures	3	98	98.33	98.99	98	98.5

4.1.3 Discussion

The proposed solution utilized a simple formula for data normalization that is not dependent on any specific dataset. It just contains variables for thresholds to eliminate artifacts that are dependent on the measuring device. This approach ensures that data preparation before using the CNN model has low computational complexity. However, there are some limitations that need to be addressed.

Nevertheless, there are certain limitations which are needed to check. To reduce computational complexity, a noise reduction algorithm was not implemented. Classification results were not devalued on tested datasets, but functionality is not guaranteed in all approach applications. and there may be cases where the environment requires deeper preprocessing due to 50Hz noise, etc. In the next point, normalization without a global threshold provides variability for model setting, but only with manual intervention. Experiments for thresholds were done by histograms instead of z-score normalization, where artifacts are only reduced rather than suppressed. The last issue corresponding with CAD systems on this basis is the performance measuring of the CNN instead of k-fold cross-validation. However, this can be replaced by data augmentation into a sufficiently large dataset.

When it comes to automated detection of health issues, CNN models have several advantages. The most significant advantage is that CNNs do not require the use of traditional tasks

in a conventional flowchart, such as pre-processing, feature extraction, and feature ranking. These tasks typically require expert knowledge, which is not necessary for designing a CNN. Instead, the CNN automatically extracts features by modifying filters within convolutional layers and weights for transitioning between layers during model training. This feature can save computational time and memory, depending on the batch size. However, it is important to note that too many big batches can lead to decreased model performance. Additionally, the CNN model is not independent of expertly-known pattern detection, such as P waves, T waves, and R peaks in ECG or the cardiac cycle in BCG, as convolutional filters search for patterns throughout the entire signal.

The results of using CNN models for automated detection lead to the conclusion that the designed solution is a suitable tool. Furthermore, the reduction in complexity allows for deployment options on devices with limited computing power or as a server implementation for the parallel detection of multiple patients. This advantage is especially important as it can improve the efficiency of healthcare providers in diagnosing and treating patients. By reducing the complexity of the model, it can be deployed on a wider range of devices, making it accessible to more people.

The detailed view of the existing work on CAD for different types of arrhythmias is shown in Table 4.6. The presented performances were measured on the classification of all four classes except [98], where only normal and A_{fib} classes were used. In the case of used data, other approaches analyzed other available databases like European ST-T Database (EDB), MIT-BIH Normal Sinus Rhythm Database (NSRDB), and Creighton University Ventricular Tachyarrhythmia Database (CUDB) Some articles are based on R-peak detection [3, 26]. However, needs long segments for a finding of the R-peak or QRS complex which makes it not possible to real-time classification. Above that, denoising methods are used for smoothing the signal [3, 5, 26, 63]. There are approaches where noise can have a big impact on the final system result. In the case of CNN, raw data can have worse Acc but is still within acceptable limits. Moreover, if the data are clearly different, the model's performance can be almost the same. The next problematic issue is separate feature extraction, feature ranking, and classification [3, 26, 71], which require knowledge of all different algorithms for the right use. Acharya et al. [5] and Xia et al. [98] is most close to this approach. Nevertheless, Z-score normalization depends on knowledge of all datasets to compute the mean and standard deviation. In the second case, wavelets are useful, like feature extractors too, so in

Table 4.6: Selected studies of the detection of arrhythmia using ECG data from various PhysioNet databases [32]

Source	Approach	Classification	Performance (%)	Data used
Current [32]	CNN with normalization	CNN	Acc = 98.45 Sen = 99.87 Spec = 99.27	AFDB MITDB VFDB
Current [33]	CNN with CWT	CNN	Acc = 97.78% Sen = 99.76% Spec = 98.82%	AFDB MITDB VFDB
[5]	CNN with Z-score	CNN	Acc = 92.50 Sen = 98.09 Spec = 93.13	AFDB MITDB VFDB
[98]	STFT with CNN	CNN	Acc = 98.63 Sen = 98.79 Spec = 97.87	AFDB
[78]	Spectogram with CNN	CNN	Acc = 97.23	AFDB EDB NSRDB VFDB
[26]	RQA	DT, RF, rotation forest	Acc = 98.37	AFDB CUDB MITDB
[3]	Thirteen nonlinear features with ANOVA	KNN with DT	Acc = 97.78 Sen = 99.76 Spec = 98.82	AFDB CUDB MITDB

combination with CNN are redundant, network input has higher resolution, and the CNN model must be more complex with a bigger number of neurons. In summary, the CNN model with normalization depends on knowledge of ECG characterization for each class, not on the dataset nor on several different methods. The objective show the robustness of CNN architecture, which can replace some processes of traditional CAD system flowchart. It could reduce the computational complexity of arrhythmia detection and dependency on the used dataset. This, in total, could provide a useful easy implementation for the practical medical environments for real-time decision support.

Moreover, a comparison of the EEG CAD system with other journal articles is shown in Table 4.7 for the Bonn dataset. The achieved Acc is comparable to the best results obtained by other methods. Unlike the presented solution, which divides the sample into smaller blocks with the following voting, all presented articles process samples with 4097 values as a single input. As a result, the architecture requires fewer inner parameters, implying

Table 4.7: Selected studies of seizures detection on Bonn EEG dataset [24]

Author	Approach and Classification	Performance (%)
Current [24]	normalization + CNN	Acc = 98.33 Sen = 98.5 Spec = 98
[58]	SSTFT + FKNN	Acc = 99.18 Sen = 99.77 Spec = 99.80
[12]	Entropy based features	Acc = 97.7
[17]	Multiscale spectral features + RF	Acc = 98.6 Sen = 98.99 Spec = 99.12
[7]	Z-score, CNN	Acc = 88.67 Sen = 95 Spec = 90
[102]	STFT + mConvA	Acc = 93.97
[60]	STFT + CNN	Acc = 99.33 Sen = 99.16 Spec = 100

less computational time per input with a greater number of classifications. From a research standpoint, the solution does not provide the necessary optimization. However, it is crucial to consider the application perspective of the point. A system that works with a 23.6 seconds length of data without sliding window implementation may provide significant latency of patient condition updates. This limitation is eliminated in the presented solution, which can update the patient's condition without any delay.

4.2 Data fusion

The fusion methodology to reduce the complexity of input and redundant information is presented in the following section. The solution presented in this section has been tested in both multi-channel and time series datasets with known triggers. Furthermore, it has been compared to other approaches from the literature.

The presented solution offers a novel input complexity reduction approach, essential for efficient and accurate data analysis. By removing redundant information, the proposed methodology could lead to improved performance in various applications, including signal processing and data analysis.

The testing of the solution in both multi-channel and time series datasets with known

triggers demonstrates its versatility and potential applicability to various data types. The comparison with other approaches from the literature further highlights the advantages of the presented methodology over existing approaches.

4.2.1 Averaging

As mentioned, multiple channels need to be processed, unlike the previous experiments on ECG databases and the Bonn EEG database. To ensure that the data can be used as one-dimensional input, the channels were merged into a single vector. The decision to average the values at the same timestamp was made because of the similarity with the average pooling layer in neural networks. However, the number of channels per person was different, and a static kernel size would not have resulted in a one-dimensional output for all inputs. As a result, the classical layer was not used, and averaging was done as a preprocessing task.

Beforehand, a correlation calculation was performed to determine the correlation between different channels. Based on the results, two channels were omitted. The T7-P7 and P7-T7 channels were excluded because they had a perfect negative correlation, and their average result was equal to zero, leading to the loss of information in the data. Additionally, the T8-P8 channels were excluded because they contained duplicate data. Including this channel would have led to an increase in weight compared to other channels, resulting in a bias in the analysis.

After conducting EEG data studies, the next step was to carry out BCG data fusion experiments. In these experiments, the samples obtained from the previous two procedures were averaged in the time domain. This resulted in vector input, which differs from the matrix input presented in Figure 4.3. The vector input was used to modify the model, where the first dimension of kernel size remained the same while the second dimension was removed. As a result, architecture 2 from 3.1.3 was utilized to achieve equivalent results.

4.2.2 Results

Experiments were conducted on the CHB-MIT dataset for each individual, and the average Acc, Sen, and Spec were computed across individuals by other researchers. Since the number of seizures varies across patients, k-fold cross-validation was performed using different folds based on each patient's data. The final results are presented in Table 4.8, which includes the

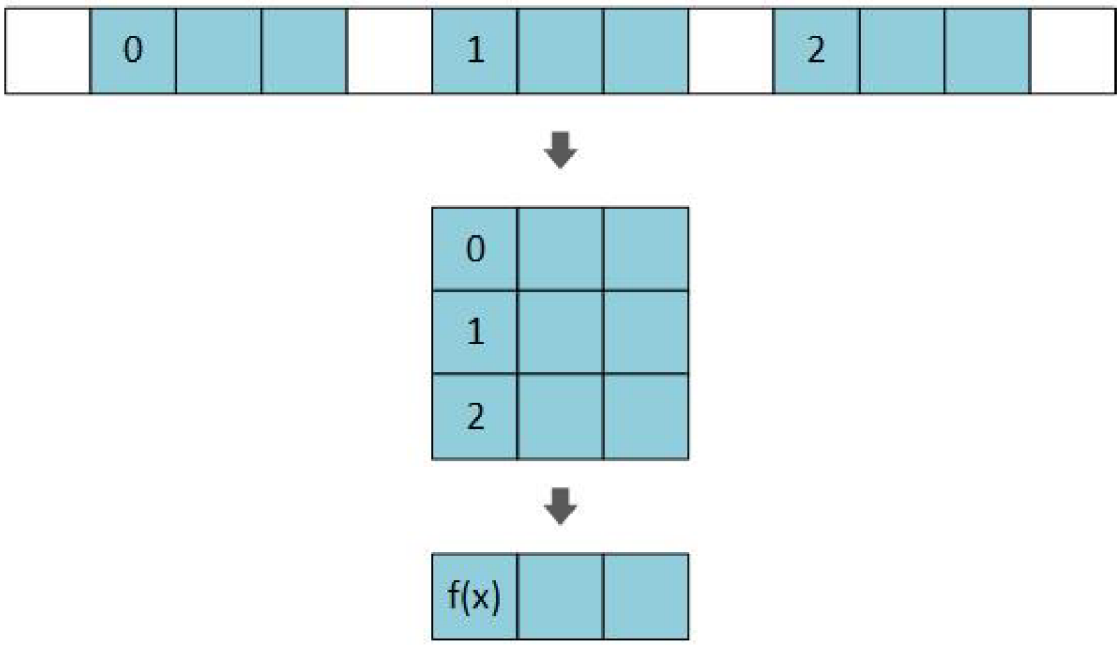

Figure 4.3: BCG fusion processing [created by the author]

overall performance of the model. Despite the unbalanced length of data and the varying number of seizures, the results were above 85%, and there was no overfitting issue. This was demonstrated by the worst training scenario, presented in Figure 4.4, which shows balanced progress over time. These findings suggest that the model performs well on the CHB-MIT dataset, even with its inherent challenges.

The best classification results of the proposed system on BCG dataset are shown in Table 4.9. Upon closer examination of the table, it is apparent that the PPV for the normal class and disorder class are 97.18% and 98.41%, respectively. This means that the probability of correctly identifying the disorder class is slightly higher than that of the normal class. It is also noticeable that 4.9% of normal samples are inaccurately classified as disorders, while 0.9% of problematic sequences are incorrectly classified as the normal class. In summary, it can be concluded that the proposed system's Acc is 98.11%. To elaborate further, these classification results suggest that the proposed system successfully differentiates between normal and problematic breathing patterns.

4.2.3 Discussion

A comparison of the CAD system with other journal articles is shown in Table 4.10. In contrast to the previous comparison, input lengths in each article are mostly unique, and

Table 4.8: Classification results of each patient on CHB-MIT EEG dataset [24]

Patient	Sen (%)	Spec (%)	Acc (%)
chb01	99.77	97.83	98.89
chb02	100	100	100
chb03	98.76	97.50	98.16
chb04	99.22	99.65	99.56
chb05	98.94	99.42	99.12
chb06	97.10	92.99	94.92
chb07	99.39	99.66	99.56
chb08	95.74	96.04	95.89
chb09	100	100	100
chb10	99.55	99.35	99.45
chb11	98.79	99.28	99.05
chb12	88.43	91.98	90.31
chb13	95.46	88.62	91.78
chb14	94.97	95.49	95.29
chb15	86.32	97.38	91.58
chb16	95.59	99.43	98.35
chb17	94.95	97.29	96.11
chb18	90.82	93.52	92.19
chb19	99.16	98.88	99.01
chb20	96.53	93.85	95.26
chb21	95.45	98.33	97.18
chb22	100	98.94	99.39
chb23	98.35	97.50	97.90
chb24	85.31	97.01	91.55
Total	96.19	97.08	96.69

Table 4.9: EEG overall classification [24]

O/P	Normal	Disordered	Acc (%)	PPV (%)	Sen (%)	Spec (%)
Normal	1243	64	98.11	97.18	95.10	99.10
Disordered	36	3973	98.11	98.41	99.10	95.10

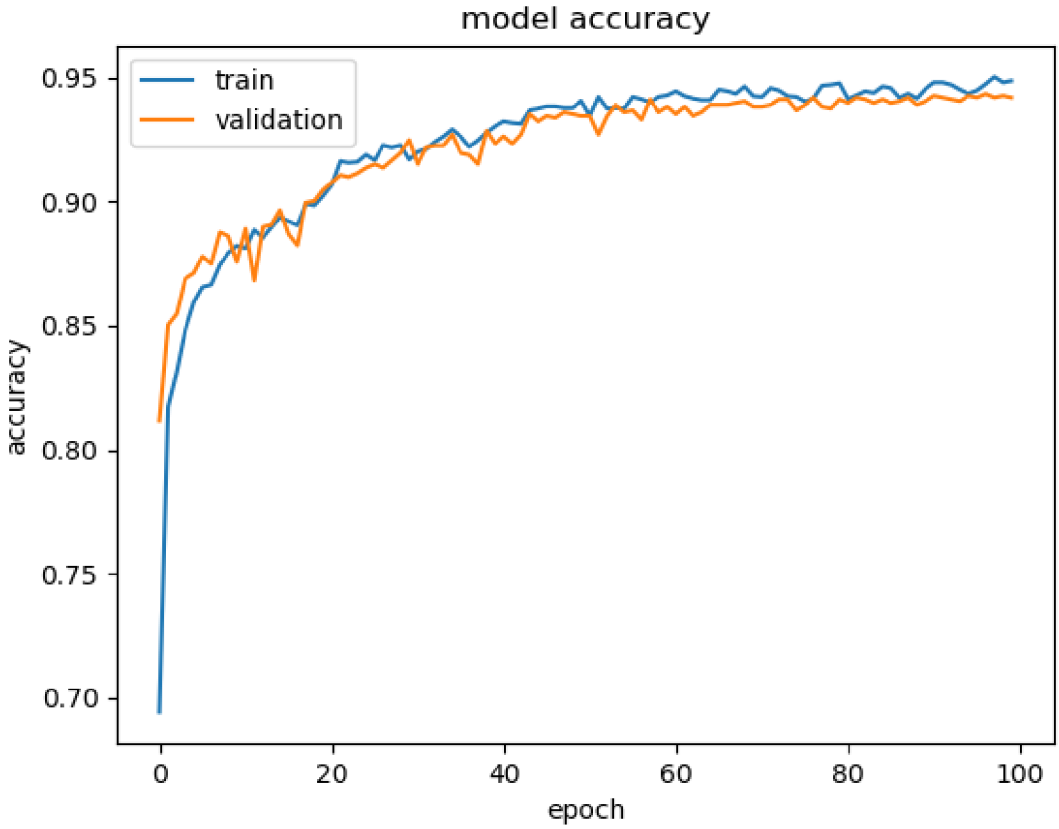

Figure 4.4: The testing and validation curves for chb24 [24]

cross-validations are not set up the same way. Furthermore, unlike the other approaches, the validation per seizure in these articles is performed without voting. However, the study conducted by Wand et al. [92] confirms the need for post-processing. They demonstrate that by transferring Sen from the segment-based level to the event-based level, the performance of the CAD system can be improved. This is achieved using a formula:

$$\mathrm{Sen}_2 = \frac{\text{number of corrected detected seizures}}{\text{number of all seizures}}. \tag{4.2}$$

Implementing it into the other presented systems should result in a reduction in the results gap. Moreover, channel fusion into vector leads to complexity reduction. As described in [31], one-dimensional CNN computational complexity in a single layer can be described as:

$$O = \mathrm{OutputSize} \cdot n_f \cdot \mathrm{Mult}(n_i, n_k) + n_f \cdot Acc(n_i, n_k) \tag{4.3}$$

where n_i, n_f, and n_k represent the number of features in the input vector, the number of filters, and the kernel size. The highest asymptotic complexity in neural network operations

is typically represented by matrix multiplication, which has a complexity of $O(n^3)$. When n layers are included in a feedforward network, the final complexity is defined as $O(n^4)$ for testing and $O(n^5)$ for training with a gradient descent task.

Although the fusion of channels does not reduce the asymptotic complexity, it can significantly decrease the computational complexity in two key ways. First, it reduces the number of weights and biases contained in the model. In the presented model, there are 10,854 inner parameters. Without fusion, the smallest possible two-dimensional CNN architecture with a kernel size of $(19, c\,h)$ could be provided, where the constant is set to be the same as in the case of the presented one-dimensional CNN, and $c\,h$ represents the number of channels. However, for $c\,h = 24$, the architecture expands by almost half to 15.667, which includes convolution and fully-connected layer operations.

The second aspect is about max-pooling layers whose output is unrelated to the number of inner parameters. However, the output size from the previous convolution layer in combination with the kernel size represents the complexity of the necessary calculations. It excludes inner parameters for fully connected layers, which total 6.651, so the number of related parameters is more than doubled in two-dimensional CNN, from 4.023 to 10.010. Furthermore, several methods are using complex preprocessing methods, such as STFT with complexity $O(n \cdot log(n))$, and increasing the dimension, instead of normalization with $O(n)$. The results lead to the conviction that the designed solution represents a suitable tool. Moreover, complexity reduction allows for deployment options on devices with limited computing power or as a server implementation for parallel detection of multiple patients.

A comparison of BCG system performance with other articles is shown in Table 4.11. A significant difference is the type of sensors used for data measuring. A few studies built a system on ECG signals for the detection of sleeping apnea. Others used a combination of ECG as a complementary device to BCG, or only a BCG measuring approach. Thus, BCG sensors are placed related to body position, such as piezoelectric foil under the body positioned on the back. In the proposed approach, BCG sensors are positioned into the measuring beds; hence, the signals processed by Cartan curvatures are independent of body position. Furthermore, fusion processing produced better results than two-dimensional inputs. Unlike EEG, BCG does not measure multiple channels at the same time, but rather more one-channel samples with time ordering. It results in a higher correlation between input rows, and data fusion does not result in as much information loss as the EEG.

Table 4.10: Selected studies of seizures detection on CHB-MIT EEG dataset [24]

Source	Approach and Classification	Performance (%)
Current [24]	normalization + CNN	Acc = 96.99 Sen = 97.06 Spec = 96.89
[34]	GAN+1DCNN	G-Mean = 96.15 Sen = 93.53 Spec = 99.05
[92]	S-1D-CNN	Acc = 99.73 Sen = 90.09 Spec = 99.81
[58]	SSTFT + FKNN	Acc = 98.99 Sen = 98.53 Spec = 99.27
[10]	adaptive STFT+LDA	Acc = 98.81 Sen = 98.44 Spec = 99.19
[104]	DWT + SVM	Acc = 96.15 Sen = 93.53 Spec = 99.05
[29]	Channel selection + KNN	Acc = 85 Sen = 86.04 Spec = 83.78
[17]	Multiscale spectral features + RF	Acc = 98.9 Sen = 98.12 Spec = 99.17
[65]	GAN	Acc = 95.06 Sen = 95.38 Spec = 94.33
[56]	Wavelets, EMD + SVM	Acc = 97.49 Sen = 97.34 Spec = 97.50
[103]	Nullcline Feature + LDA,NN	Acc = 97.49 Sen = 97.34 Spec = 97.50

Aside from the complete unobtrusiveness of the system, there are two major advantages in comparison with recent studies. Cartan curvatures contain information not only about pulse arrival time but also about the complex hemodynamics of the person [52]. In the first work [21], the focus has been on the pulse arrival time at one specific point, but later it was extended in employing CNN at the whole beat-to-beat Cartan curvatures. The approach brings both better results and removing of unnecessary feature extraction. These could open various topics in the future with a focus on the study of Cartan curvatures without the use of ECG thus enabling full automation of the system and studying other aspects of human hemodynamics. Secondly, studying the whole Cartan curvatures offers the possibility of achieving greater precision in the system, with fewer errors due to falsely detected pulse arrival times. The method is also effective with people in different positions, which provides indirect proof that Cartan curvatures are invariant under rotational and translational changes of the human body on the bed. Additionally, since there is no need to precisely detect pulse arrival times, the computational power needed for preprocessing has decreased. Furthermore, there are additional calculations that can be performed with even greater performance without the computation of pulse arrival time, with Cartan curvatures serving as input.

Furthermore, it is evident that the fusion process can lead to complexity reduction and performance improvement. This has been demonstrated through a comparison of results in [22] and [23] before and after the averaging process. This observation highlights the possibility of processing a different number of time-ordered samples without modifying the CNN architecture and finding the ideal interval to achieve the best Acc, Sen, and Spec results. Moreover, the ability to optimize the number of time-ordered samples processed without modifying the CNN architecture offers greater flexibility and adaptability to different datasets.

4.3 CNN

The last section of the practical part focuses on the possibilities of reducing and utilizing CNN. Structurally, it is divided into two areas that describe three issues. The first part of the section verifies the hypothesis of reusability, while the second part describes the mutual interdependence between the reduction of frequency and architecture.

Table 4.11: Selected studies of the detection of breathing disorders [created by the author]

Source	Approach	Classification	Types of sensors	Performance (%)
Current	Averaging of [23]	CNN	BCG	Acc = 97.25 Sen = 93.41 Spec = 98.25
Current	Averaging of [22]	CNN	BCG	Acc = 98.11 Sen = 95.10 Spec = 99.10
[23]	Cartan curvatures with Euclidean length trigger	CNN	BCG	Acc = 96.37 Sen = 92.46 Spec = 98.11
[22]	Cartan curvatures with normalization	CNN	BCG	Acc = 98.00 Sen = 94.26 Spec = 99.22
[21]	Cartan curvatures with CWT on pulse arrival	CNN	BCG	Acc = 89.35 Sen = 86.35 Spec = 91.22
[76]	Adaptive thresholding	Statistically	BCG	Sen = 24.24 Spec = 85.88
[59]	Threshold-based division	NN	BCG	Acc = 94.6
[106]	STC-Min	SVM	BCG	Acc = 90.46
[100]	Locally Projective Noise Reduction	Heuristic	BCG	Acc = 92.7 Sen = 99.5
[41]	Tunable-Q factor wavelet transform	Adaptive boosting	ECG	Acc = 87.33 Sen = 81.99 Spec = 90.72
[74]	Linear and non-linear features	RF	ECG	Acc = 91.77 Sen = 89.53 Spec = 93.43

The hypothesis of reusability has been tested in the first part of the section, highlighting the potential of CNN to be reused in different applications. This emphasizes the versatility and adaptability of CNN, making it a valuable tool in various fields of research.

The second area offers a novel approach to complexity reduction, which is essential for efficient and accurate data analysis. The reduction of frequency and architecture simultaneously allows for greater adaptability and flexibility in different datasets, and without performance loss.

Table 4.12: ECG and EEG combination confusion matrix [created by the author]

O/P	Normal_{ECG}	A_{fib}	A_{fl}	V_{fib}	Normal_{EEG}	Preictal	Seizure
Normal_{ECG}	3529	15	13	4	0	6	0
A_{fib}	18	19147	47	21	0	10	29
A_{fl}	13	83	1403	5	0	6	8
V_{fib}	0	35	3	886	2	28	12
Normal_{EEG}	0	0	0	1	769	21	9
Preictal	10	8	4	26	21	719	12
Seizure	7	23	21	13	8	12	716

Table 4.13: ECG and EEG combination overall classification [created by the author]

TP	TN	FP	FN	Acc (%)	PPV (%)	Sen (%)	Spec (%)
4298	23277	69	79	99.46	98.42	98.19	99.7

4.3.1 Model reusability

The results of the same CNN model are presented in sections 4.1 and 4.2, which are related to the hypothesis about architecture reusability described in section 3.6.1. However, it is important to note that well-known pre-trained models are prepared in a wide range of classes, and an initial experiment was conducted by combining different health issues measured by different devices. Specifically, ECG data in combination with EEG data from the Bonn University database were chosen because they had the same length of input data.

It is worth noting that the CHB-MIT database, which includes other EEG data and is commonly used for cross-validation, was not used in this experiment. This decision was made because the EEG data from the two databases were not labeled by the same scenario, and the Bonn University database contained more classes.

The findings of this experiment are shown in Tables 4.12 and 4.13. The CNN model utilized in the ECG data demonstrated that the user architecture can categorize even this combination of ECG and EEG data, implying that the amount of input data and the number of identified classes increased without any changes to the internal structure of the CNN.

4.3.2 Frequency and architecture reduction

The experiments on frequency analysis were conducted on EEG, ECG, and BCG. The results of the EEG data analysis are presented graphically in Figure 4.5. The analysis showed a slight improvement in Acc for 225Hz classification compared to 200Hz classification. However,

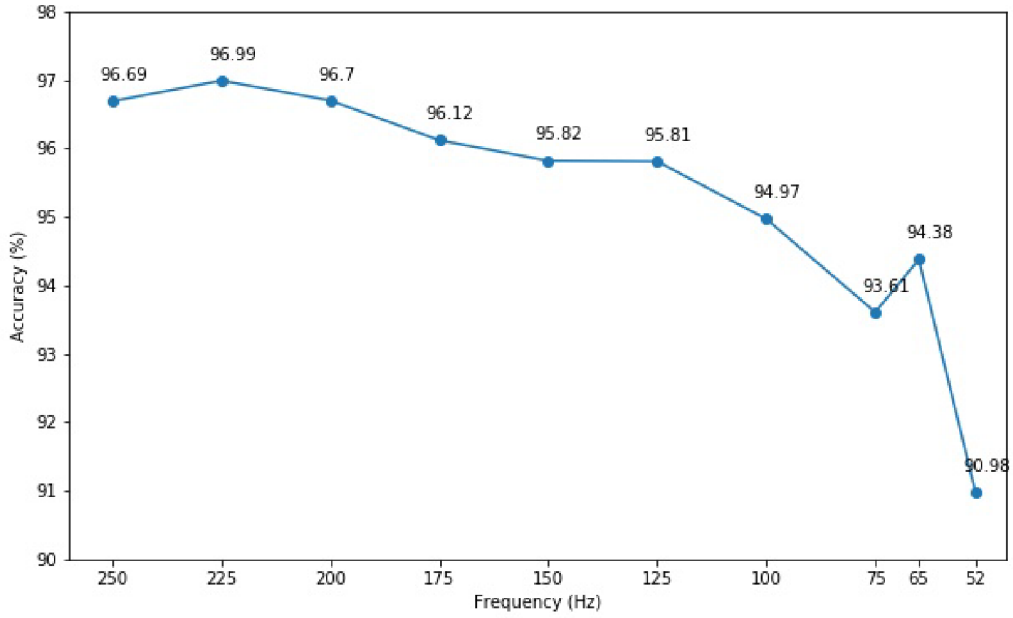

Figure 4.5: EEG Acc of different frequencies [created by the author]

the Sen was found to be higher for 225Hz, which led to a decrease in Spec. As the frequency was reduced further, there was a gradual decline in performance. Surprisingly, there was a peak-down in performance for the 75Hz experiment.

The various resample values were tested to determine the maximum possible resample without architectural redesign. The highest possible resample value that could be tested was 52Hz. With this resample value, the transmission output from the fifth to the sixth layer was 1x11 instead of 50x11. Furthermore, other down-sampling resulted in nonpositive values. Despite these limitations, the proposed methodology maintained a performance level of over 91% even in the worst-case scenario, which indicates its practical applicability.

Downsampling the data to 50Hz reduces the number of inner parameters in the CNN by an average of 800 values. However, it's important to note that this operation involves other processing steps. Reducing the first frequency (which typically provides the best Acc, Sen, and Spec) may not necessarily reduce time complexity, depending on the specific device used. Despite this, the results obtained through downsampling do correlate with the image classification discussed earlier in this subsection and provide valuable insights for measuring device needs. This knowledge can be used to optimize the performance of CNNs on different devices.

The experiments conducted on both ECG and EEG data utilized the same CNN architec-

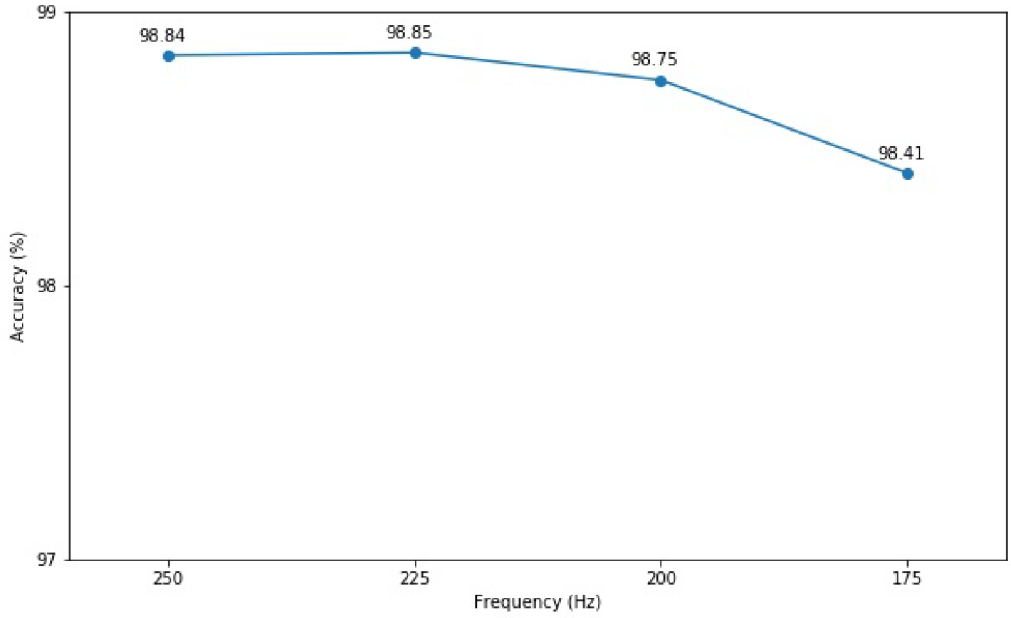

Figure 4.6: ECG Acc of different frequencies [created by the author]

ture, which allowed for the calculation of inner parameters for different frequencies in both cases. The results of the ECG experiments are presented in Figure 4.6. Notably, the highest performance results were achieved at a frequency of 225Hz. There are two possible reasons for this outcome.

The first is frequency suitability, which balances redundant resolution in higher frequencies with information loss in lower ones. This means that the 225Hz frequency is optimal for capturing the necessary information in the ECG signals without sacrificing too much resolution. The second possibility is that there is a correlation between the frequency used and the CNN model's architecture, which was ideally designed for this specific input form.

Due to BCG measurement containing data on 1KHz, Figure 4.7 depicts the successive downsampling from the highest option until obvious Acc decreases. The findings support a frequency suitability theory rather than architectural influence, but the statistical population is too small to make a final hypothesis decision. Nonetheless, promising experiments open up new avenues for future research.

The following tables present the results of experiments on model complexity, including the number of blocks, filters, frequency, and inner parameters. The best outcomes for each architecture are shown in bold. However, evaluating a model solely based on Acc and complexity is insufficient. It becomes questionable when an increase in Acc of only a

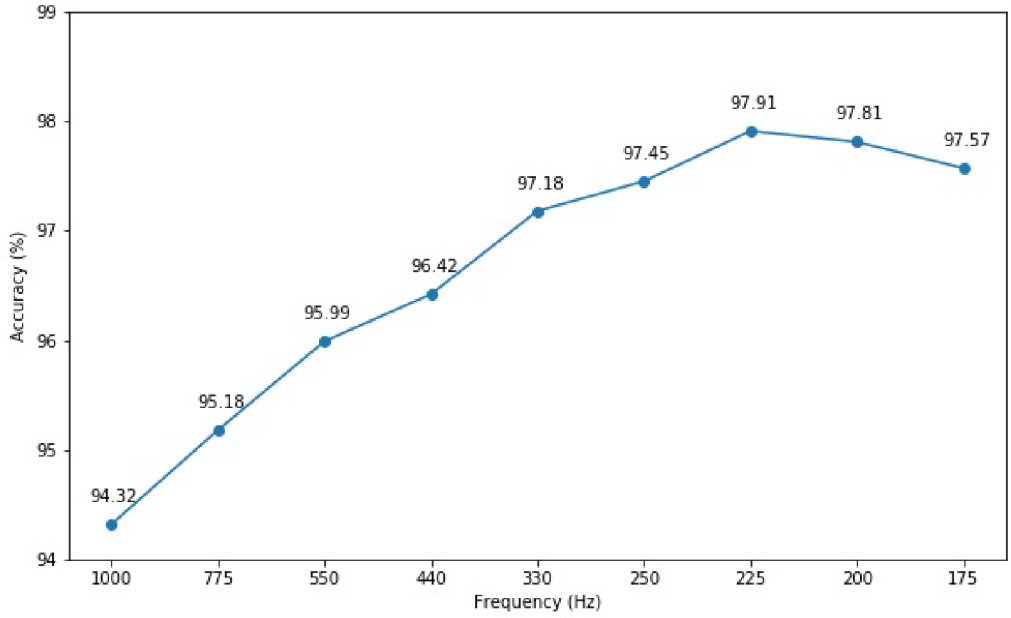

Figure 4.7: BCG Acc of different frequencies [created by the author]

tenth of a percentage requires hundreds or thousands of additional inner parameters. To address this issue, we propose using event-based level Sen as a performance comparator, as suggested by Wang et al. [92]. By applying the equation shown in Equation 4.2, we can obtain metrics that allow for a clearer comparison of models and aid in decision-making regarding adding weights and biases.

Due to the high-frequency measurement, we initially tested the architectural analysis using BCG data. Our findings for individual experiments are presented in tables 4.14 and 4.15 for CNNs with two to five blocks, respectively. For the two-block architecture, the highest Acc was achieved using the maximum set of filters. This model contains over 60k parameters, which is fewer than in networks with more blocks, but still achieved high Acc.

In the three and four-block experiments, we found that similar parameters were needed to achieve peak Acc. However, despite having the same model complexity, the four-block architecture outperformed the three-block architecture in terms of both Acc and Sen_2. In fact, the four-block architecture provided the highest Acc among all the models tested.

For our final BCG experiment, we increased the model complexity by almost twice. Still, the resulting Acc increase was only 0.13% compared to a similar number of parameters in the best three- and four-block architectures. This suggests that increasing model complexity beyond a certain point does not necessarily translate to significant improvements in Acc.

Table 4.14: BCG CNN results for 2 and 3 blocks [created by the author]

blocks	2				3			
filters	freq	Acc	Sen_2	params	freq	Acc	Sen_2	params
10	600	92.09	74.01	18148	150	94.13	76.78	4098
15	225	94.66	77.68	11108	150	96.65	82.14	8378
20	100	95.75	83.03	8458	150	97.85	81.25	14158
25	250	96.45	75.00	23338	200	98.56	83.92	23238
30	100	97.29	80.35	15968	150	98.87	79.46	30218
35	100	98.04	78.15	20548	150	99.07	79.46	40498
40	100	98.52	77.67	25678	225	98.83	77.67	56598
45	100	98.33	81.25	31358	150	98.97	79.46	65538
50	100	98.5	71.42	37588	**150**	**99.16**	79.46	**80338**
55	100	98.73	77.67	44368	100	99.04	80.35	92658
60	100	98.69	80.35	51698	100	99.19	80.35	110078
65	**100**	**98.85**	77.67	**59578**	150	99.12	79.46	133678

Table 4.15: BCG CNN results for 4 and 5 blocks [created by the author]

blocks	4				5			
filters	freq	Acc	Sen_2	params	freq	Acc	Sen_2	params
10	225	95.2	77.68	4728	400	95.78	76.78	5718
15	250	97.09	79.46	10328	400	97.61	81.25	12458
20	225	98.16	81.25	17618	369	98.48	82.14	21558
25	200	98.43	78.57	26538	400	98.66	82.14	33738
30	400	98.54	81.25	42668	369	98.72	80.35	47918
35	200	98.72	80.35	51488	369	98.83	72.32	64998
40	225	98.92	78.57	67998	369	99.06	81.25	84678
45	**225**	**99.3**	83.03	**85718**	400	98.91	77.68	107498
50	225	99.15	85.71	104288	400	99.01	83.03	132438
55	200	99.06	75.89	125988	**400**	**99.19**	75.89	**159978**
60	200	99.24	81.25	149738	400	99.14	80.35	190118
65	200	99.23	81.25	175538	369	99.16	78.57	222078

The results of experiments conducted on ECG databases have been tabulated in a manner similar to that of the BCG, as presented in tables 4.16 and 4.17. While the Acc peaks of the architectures for ECG and BCG are similar in terms of the number of parameters, the former exhibits better Acc results. This holds true not only for the best results but also for architectures with almost the same number of neurons. Interestingly, the ideal frequency for ECG is around 225Hz and 250Hz, which is significantly higher than the frequency that resulted in the top Acc for several BCG experiments, i.e., 100 Hz. Given the experimental design, in the instance of ECG, Sen across events rather than samples adds no benefit because:

Table 4.16: ECG CNN results for 2 and 3 blocks [created by the author]

blocks	2			3		
filters	freq	Acc	params	freq	Acc	params
10	225	97.99	13614	225	98.79	8564
15	250	98.33	23554	250	99.05	16144
20	250	98.58	32484	250	99.14	24504
25	225	98.5	38064	225	99.25	32564
30	250	98.51	51994	250	99.26	45724
35	**250**	**98.66**	**62574**	250	99.19	58584
40	250	98.58	73704	225	99.28	70064
45	250	98.52	85384	**225**	**99.33**	**85564**
50	250	98.53	97614	250	99.32	106164
55	225	98.64	101814	250	99.28	125024
60	250	98.45	123724	250	99.26	145384
65	225	98.63	127464	200	99.25	157884

Table 4.17: ECG CNN results for 4 and 5 blocks [created by the author]

blocks	4			5		
filters	freq	Acc	params	freq	Acc	params
10	250	99.24	6794	250	98.99	6104
15	250	99.33	13234	250	99.34	13024
20	250	99.38	21724	250	99.43	22544
25	250	99.46	32264	250	99.42	34664
30	250	99.48	44854	250	99.5	49384
35	250	99.49	59494	250	99.48	66704
40	250	99.49	76184	250	99.54	86624
45	250	99.51	94924	250	99.52	109144
50	250	99.48	115714	**250**	**99.55**	**134264**
55	250	99.52	138554	250	99.46	161984
60	**250**	**99.53**	**163444**	250	99.52	192304
65	250	99.52	190384	250	99.51	225224

- There is more than one database and the data is measured in several ways.
- Normal sections and with issues swap often, hence, unlike EEG and BCG, the same difficulty as with Acc arises here.
- The database has more cardiac issues than just two classifications (positive and negative), where normal data represents a smaller group and emphasizes the preceding point.

The EEG experiments on a selected patient, labeled as chb24, are presented in the same manner as in previous articles due to the setup of experiments carried out therein. This

Table 4.18: EEG CNN results for 2 and 3 blocks [created by the author]

blocks	2				3			
filters	freq	Acc	Sen_2	params	freq	Acc	Sen_2	params
10	150	83.34	91.67	9148	225	89.61	91.67	8538
15	150	84.21	100	14528	225	90.99	100	15038
20	150	84.64	100	20458	200	91.36	100	21598
25	150	85.14	100	26938	225	92.6	100	32538
30	150	85.09	100	33968	225	93.23	100	43538
35	150	85.71	100	41548	225	92.94	100	56038
40	150	85.98	100	49678	**250**	**93.92**	100	**72918**
45	150	86.56	100	58358	225	93.27	100	85538
50	150	86.92	100	67588	250	93.17	100	106138
55	**150**	**86.97**	100	**77368**	250	93.05	100	124998
60	150	86.83	100	87698	225	93.05	100	141038
65	150	86.68	100	98578	250	93.72	100	167218

Table 4.19: EEG CNN results for 4 and 5 blocks [created by the author]

blocks	4				5			
filters	freq	Acc	Sen_2	params	freq	Acc	Sen_2	params
10	225	91.17	91.67	6408	225	90.43	91.67	5838
15	225	93.31	100	12668	250	92.94	100	12638
20	225	94.29	100	20978	225	93.15	100	22038
25	250	94.28	100	32238	**225**	**94.56**	**100**	**34038**
30	225	95.03	100	43748	250	94.23	100	49358
35	250	95.18	100	59468	250	93.54	100	66678
40	225	94.91	100	74718	200	91.08	100	84678
45	250	94.84	100	94898	250	93.2	100	109118
50	250	94.32	100	115688	250	85.14	100	134238
55	250	94.48	100	138528	250	87.53	100	161958
60	**250**	**95.3**	**100**	**163418**	225	83.88	100	190838
65	250	94.77	100	190358	225	86.28	100	223638

decision was made based on the worst individual results observed in the segment-based level Sen analysis presented in Table 4.8. The results of the analysis revealed that the block number had the biggest impact on the final Acc comparison.

Furthermore, it was observed that despite the implementation of batch normalization and dropout techniques, models with too many parameters tended to overfit. This phenomenon was more prevalent in the design of the deepest architecture. It is important to note that overfitting occurs when a model is trained on a limited set of data, or the architecture's initial setup and optimizer are not made properly.

In the Sen_2 experiments, the results for all the blocks were found to be the same. As a

result, we decided to provide information about the optimized architecture for each patient separately to achieve the best Sen_2 performance without using redundant parameters. For this purpose, Table 4.20 contains a detailed summary of the optimized architecture used for each patient in the experiment. It is important to note that these experiments were conducted using an architecture with four blocks, which provided the best Acc for all BCG, ECG, and EEG data.

In our study, we observed a strong negative correlation between the Acc of the experiment conducted in [24] and the number of filters required to provide maximal Sen_2. This finding was quite surprising, and it suggested that using fewer filters can result in higher Acc in the detection of seizures.

One particular result that stood out was in the case of chb12, where the measurement Acc was 90.31%. Interestingly, it was found that only one filter was needed to achieve this high level of Acc. However, despite the high Acc, we observed that the Sen and Spec values (as shown in Table 4.8) were relatively low, which resulted in false alarms in the case of normal data and more separate alarms in the case of seizures.

4.3.3 Discussion

Future research can explore various directions. In terms of model reusability and the fact that patients can suffer from multiple healthcare issues at once, it is essential to use the CAD system for decision support in all available cases. Moreover, there are other types of time series data that can be integrated into the system, such as galvanic skin response for epilepsy detection [64], electromyography signal for robotic interaction [80], and neuromuscular disorders [49].

However, the main challenge for researchers is to collect a diverse range of datasets that cover as many health issues as possible. Another limitation is the need for various CAD models for each disease. Despite these challenges, the presented methodology can be applied to different topics, and researchers can collect different kinds of data that are normalized based on the measuring device and trained for future deployment.

In conclusion, future research can take several different directions. Researchers can overcome the current limitations by collecting diverse datasets, exploring different types of time-series data, and using deeper data analysis to enhance the system's performance.

To take the research to the next level, deeper data analysis for the CNN classification

Table 4.20: Architecture optimization of each patient on CHB-MIT EEG dataset [created by the author]

Patient	No. seizures	Sen_2 (%)	Acc (%)	filters
chb01	7	100	98.89	2
chb02	2	100	100	1
chb03	7	100	98.16	2
chb04	3	100	99.56	2
chb05	5	100	99.12	1
chb06	7	100	94.92	3
chb07	3	100	99.56	1
chb08	5	100	95.89	1
chb09	3	100	100	2
chb10	7	100	99.45	3
chb11	3	100	99.05	1
chb12	13	100	90.31	1
chb13	8	100	91.78	7
chb14	7	100	95.29	2
chb15	14	100	91.58	4
chb16	6	100	98.35	3
chb17	3	100	96.11	2
chb18	6	100	92.19	12
chb19	3	100	99.01	1
chb20	6	100	95.26	3
chb21	4	100	97.18	3
chb22	3	100	99.39	6
chb23	3	100	97.90	3
chb24	12	100	91.55	9

can be explored. This approach will reduce the complexity of the system and enable better decision support. The possibilities of the architecture of neural networks have been analyzed to a certain level, which does not entirely cover all aspects that neural networks can contain. The number of neurons employed in the fully-connected layers is one of the CNN characteristics that remained constant throughout trials. A relationship between the ratio and preceding layers should be examined, where adding neurons to fully connected produces a reduction in CNN number of filters to preserve trainable parameter count and avoid overfitting. Another static variable is the kernel size for each block. These values were examined in ECG testing, but it doesn't mean that other sizes for other data types won't result in better performance. ECG variations are mostly defined by the QRS complex, which is only a portion of the input. The difference between a normal signal and seizure detection, on the other hand, is included in the entire sample.

During the course of architectural reduction tests, it was discovered that correlation in blocks with trainable parameter count peaks when Acc is not improving. As future work, the process partially involves trial-and-error analysis, which calls for the automation of an appropriate methodology. One possible solution is to conduct a different analysis of signal data between individual classes. This involves analyzing the amplitudes of individual samples, for which entropies can be used [2]. The concept is to calculate different entropies that describe the vector data from various perspectives. These entropies must be compared intra-group within a class and inter-group within all the data to analyze the level of their dissimilarity, thereby determining the necessary filter values for successful classification. By automating this process, researchers can save time and effort optimizing their models, ultimately leading to more efficient and accurate results.

In addition to this, it is becoming increasingly important to use the appropriate techniques to tackle issues related to "black-box" algorithms. It is essential to test the performance of these models through various approaches to ensure that they are interpretable, explainable, and robust. Machine learning explainability aims to provide insight into how models work from input to output, and it can be categorized into two types: local and global.

Local interpretability analyzes individual predictions made by a model and is closely linked to a set of features that must remain consistent. Amit et al. [27] introduced the ProfWeight approach to model explainability. This approach converts the high test Acc of a deep neural network into the poor test Acc of a shallow network.

A deeper approach to local interpretability is local interpretable model-agnostic explanations (LIME), which was developed by researchers at the University of Washington. LIME measures the output results of various sub-parts performed around a certain prediction. As the number of dimensions increases, it becomes increasingly difficult to maintain local authenticity for such models.

In contrast to local models that examine the behavior of the model for a specific input, global models examine the behavior of the model for a wide range of inputs. This includes the impact of individual-specific input on the classification results. To measure this impact, accumulated local effects (ALE) is a technique that can be used. ALE analyzes how the model output changes as a specific feature changes while keeping all other features constant. The difference in the model's anticipated output due to the change in the feature value is computed using ALE. This is then integrated over the feature's range to visualize the impact

of the feature on the model output. By analyzing the ALE charts, one can determine how the model makes its predictions and identify the magnitude and direction of a feature's influence on model output.

Another technique for measuring the effect of a feature on model prediction is partial dependence (PD). Like ALE, PD assesses the change in model output as a feature's value changes while keeping all other characteristics constant. However, unlike ALE, PD computes the average effect of the feature over all possible values, instead of integrating over the feature's range. PD plots can identify trends and interactions between features, which can help explain how the model predicts.

These approaches can be used in vital data classification to determine whether the results are based on exact features, noise, or other aspects. By using ALE and PD techniques, we can identify the most influential features and explain how the model predicts.

5

Fulfillment of Objectives

The goal of this dissertation was to propose improvements to the computer processing of signal data in the field of informatics, specifically in a hospital setting. Raw data was thoroughly analyzed to extract important components for further target selection. The use of CNN designs for data classification, which can reduce the need for multiple procedures prior to classification, was explored. This technique resulted in a more accurate and reliable classifier, while also reducing the computing complexity and time required for classification.

The objectives of the study were described in chapter 2, where the primary objective was to enhance the efficiency of the classification system. The proposed solution's flowchart is illustrated in Figure 1.1, which was achieved through the pursuit of three goals.

The initial goal involved the preparation of raw data into a suitable format, as outlined in section 3.4, with results presented in section 4.1. The aim is to investigate the potential of processing tasks in combination with a CNN classifier to reduce computing time or eliminate certain processes, resulting in system reduction. Research findings were published in methodology [32], where the combination of proper normalization and CNN architecture resulted in the omission of complex preprocessing and feature extraction tasks. The methodology was compared with existing literature reviews, including prior research [33], which utilized CWT extractor and demonstrated information redundancy with no improvement in results and a more complicated CNN architecture.

The secondary goal contained the use of a data fusion procedure to reduce complexity and dependence on specific channels. Section 3.5 provides a discussion of the current solutions, while the presentation of results can be found in section 4.2. The network architecture was simplified by one dimension without compromising its ability to detect health risks. Two types of input were tested for the fusion process. The first consisted of multi-channel EEG

data, for which results were previously published in [24]. The proposed methodology was then applied retrospectively in conjunction with previous research approaches, as outlined in [22, 23]. The approaches involved the use of ordered time-series data, and the fusion process resulted in even better performance while requiring fewer internal parameters.

The final goal covered an analysis of input frequency, with the theory and hypothesis presented in section 3.6 and the evaluation provided in section 4.3. An architecture analysis was also conducted. Frequency experiments on an EEG dataset were published in [24] and were later performed on both ECG and BCG data. The CNN architecture attempts were based on insights gained from the entire study and discussed in subsection 4.3.3, including possible future research directions.

6

Conclusion

The primary objective of the thesis was achieved through three sub-areas of research. The first sub-area involved data processing aimed at eliminating counterproductive tasks. This enhanced the system's efficiency and improved overall Acc. The second sub-area involved data fusion, which aimed to reduce the complexity of CNN by one dimension. Finally, the third sub-area involved architecture analysis, which aimed to design a suitable number of blocks with reduced filters. This was done through frequency analysis to identify the need to measure device quality, thereby ensuring the Acc of the system. All experiments were conducted using free, publicly available databases with variously labeled health problems. These experiments allowed for a comprehensive analysis of the system's performance in different scenarios and helped to validate the proposed methodology.

CAD systems are constructed using traditional flowchart procedures involving four main stages: preprocessing, feature extraction, feature selection, and classification. During our research, an investigation of these tasks in detail was performed. As a result, we presented a CNN architecture that demonstrated robustness in performance. Specifically, we found that we could skip the feature extraction step by normalizing the data based on its knowledge features. Our experiments showed that this approach led to higher performance than when using the CWT technique for feature extraction. Moreover, using normalized data resulted in a model with an input displayed as a vector rather than a two-dimensional matrix that includes useless weights and biases. This simplifies the model and reduces its computational complexity, making it more efficient.

The initial research focused on ECG data but can also implement the methodology on EEG data to demonstrate its reusability. The hypothesis has been proven that the same architecture could be used for both data types, not just the preprocessing steps, but the

entire CNN model. By doing so, the results confirm the versatility and generalizability of the approach.

Due to healthcare involving the use of various devices and channels to measure health-related data, there is a need to simplify data processing and reduce dependencies on the specific channels used. To address this issue, a data fusion process was tested to reduce complexity and improve performance in detecting health issues.

By properly setting up the network design, it is possible to reduce one dimension without sacrificing performance. This method has been experimented with using the EEG database and has been found to be effective. In fact, the method has been reused in BCG research and has resulted in increased Acc, Sen, and Spec.

When it comes to image classification, having the highest quality input resolution is not always necessary. The CNN model is designed to detect the major patterns that distinguish one class from another. To transfer this knowledge from pictures to vital data categorization, frequency reduction tests have been conducted. These tests help to determine the most relevant features to use in the model, which can reduce the amount of data needed for classification.

Furthermore, an architectural study of healthcare concerns has been conducted, which has helped identify a proper collection of blocks and filters that are correlated with the input shape. This study is important because healthcare data is complex and can vary in size and shape, depending on the source. The model can better handle this variability by identifying the appropriate blocks and filters and providing more accurate results.

All submodules mentioned in the study were compared to papers from the literature. In most cases, presented results showed equivalent or improved performance with reduced complexity. In situations where Acc, Sen, or Spec decreased, the reduction was not significant, and the benefits of the approach were discussed at length.

Specifically, we found that our approach provided several advantages over existing methods. First, the submodules were significantly simpler, making them easier to implement, reducing the potential for errors, removing unnecessary pattern duplications, and not losing classification performance. Additionally, the approach was more computationally efficient, allowing for faster processing and reduced resource usage. It makes the methodology more flexible, allowing for customization and adaptation to a wide range of applications.

Literature

[1] Ossama Abdel-Hamid, Abdel-rahman Mohamed, Hui Jiang, Li Deng, Gerald Penn, and Dong Yu. Convolutional neural networks for speech recognition. *IEEE/ACM Transactions on audio, speech, and language processing*, 22(10):1533–1545, 2014.

[2] U Rajendra Acharya, Hamido Fujita, Vidya K Sudarshan, Shreya Bhat, and Joel EW Koh. Application of entropies for automated diagnosis of epilepsy using eeg signals: A review. *Knowledge-based systems*, 88:85–96, 2015.

[3] U Rajendra Acharya, Hamido Fujita, Muhammad Adam, Oh Shu Lih, Tan Jen Hong, Vidya K Sudarshan, and Joel EW Koh. Automated characterization of arrhythmias using nonlinear features from tachycardia ecg beats. In *2016 IEEE International Conference on Systems, Man, and Cybernetics (SMC)*, pages 000533–000538. IEEE, 2016.

[4] U Rajendra Acharya, Hamido Fujita, Muhammad Adam, Oh Shu Lih, Vidya K Sudarshan, Tan Jen Hong, Joel EW Koh, Yuki Hagiwara, Chua K Chua, Chua Kok Poo, et al. Automated characterization and classification of coronary artery disease and myocardial infarction by decomposition of ecg signals: A comparative study. *Information Sciences*, 377:17–29, 2017.

[5] U Rajendra Acharya, Hamido Fujita, Oh Shu Lih, Yuki Hagiwara, Jen Hong Tan, and Muhammad Adam. Automated detection of arrhythmias using different intervals of tachycardia ecg segments with convolutional neural network. *Information sciences*, 405:81–90, 2017.

[6] U Rajendra Acharya, Hamido Fujita, Shu Lih Oh, U Raghavendra, Jen Hong Tan, Muhammad Adam, Arkadiusz Gertych, and Yuki Hagiwara. Automated identifica-

tion of shockable and non-shockable life-threatening ventricular arrhythmias using convolutional neural network. *Future Generation Computer Systems*, 79:952–959, 2018.

[7] U Rajendra Acharya, Shu Lih Oh, Yuki Hagiwara, Jen Hong Tan, and Hojjat Adeli. Deep convolutional neural network for the automated detection and diagnosis of seizure using eeg signals. *Computers in biology and medicine*, 100:270–278, 2018.

[8] Paul S Addison. Wavelet transforms and the ecg: a review. *Physiological measurement*, 26(5):R155, 2005.

[9] Shameem Akhter and Jason Roberts. *Multi-core programming*, volume 33. Intel press Hillsboro, 2006.

[10] Mohsen Amiri, Hassan Aghaeinia, and Hamid Reza Amindavar. Automatic epileptic seizure detection in eeg signals using sparse common spatial pattern and adaptive short-time fourier transform-based synchrosqueezing transform. *Biomedical Signal Processing and Control*, 79:104022, 2023.

[11] Ralph G Andrzejak, Klaus Lehnertz, Florian Mormann, Christoph Rieke, Peter David, and Christian E Elger. Indications of nonlinear deterministic and finite-dimensional structures in time series of brain electrical activity: Dependence on recording region and brain state. *Physical Review E*, 64(6):061907, 2001.

[12] Arti Anuragi, Dilip Singh Sisodia, and Ram Bilas Pachori. Epileptic-seizure classification using phase-space representation of fbse-ewt based eeg sub-band signals and ensemble learners. *Biomedical Signal Processing and Control*, 71:103138, 2022.

[13] Annushree Bablani, Damodar Reddy Edla, and Shubham Dodia. Classification of eeg data using k-nearest neighbor approach for concealed information test. *Procedia computer science*, 143:242–249, 2018.

[14] Prabal Datta Barua, Tugce Keles, Sengul Dogan, Mehmet Baygin, Turker Tuncer, Caner Feyzi Demir, Hamido Fujita, Ru-San Tan, Chui Ping Ooi, and U Rajendra Acharya. Automated eeg sentence classification using novel dynamic-sized binary pattern and multilevel discrete wavelet transform techniques with tseeg database. *Biomedical Signal Processing and Control*, 79:104055, 2023.

[15] Andrea Biasiucci, Benedetta Franceschiello, and Micah M Murray. Electroencephalography. *Current Biology*, 29(3):R80–R85, 2019.

[16] Walter F Boron and Emile L Boulpaep. *Medical Physiology E-Book*. Elsevier Health Sciences, 2016.

[17] Monisha Chakraborty, Debjani Mitra, et al. A computationally efficient automated seizure detection method based on the novel idea of multiscale spectral features. *Biomedical Signal Processing and Control*, 70:102990, 2021.

[18] François Chollet. Xception: Deep learning with depthwise separable convolutions. In *Proceedings of the IEEE conference on computer vision and pattern recognition*, pages 1251–1258, 2017.

[19] SA Chouakri, Fethi Bereksi-Reguig, and Abdelmalik Taleb-Ahmed. Qrs complex detection based on multi wavelet packet decomposition. *Applied Mathematics and Computation*, 217(23):9508–9525, 2011.

[20] Grant V Chow, Joseph E Marine, and Jerome L Fleg. Epidemiology of arrhythmias and conduction disorders in older adults. *Clinics in geriatric medicine*, 28(4):539–553, 2012.

[21] Dalibor Cimr and Filip Studnička. Automatic detection of breathing disorder from ballistocardiography signals. *Knowledge-Based Systems*, 188, 2020.

[22] Dalibor Cimr, Filip Studnicka, Hamido Fujita, Hana Tomaskova, Richard Cimler, Jitka Kuhnova, and Jan Slegr. Computer aided detection of breathing disorder from ballistocardiography signal using convolutional neural network. *Information Sciences*, 541, 2020.

[23] Dalibor Cimr, Filip Studnicka, Hamido Fujita, Richard Cimler, and Jan Slegr. Application of mechanical trigger for unobtrusive detection of respiratory disorders from body recoil micro-movements. *Computer Methods and Programs in Biomedicine*, 207, 2021.

[24] Dalibor Cimr, Hamido Fujita, Hana Tomaskova, Richard Cimler, and Ali Selamat. Automatic seizure detection by convolutional neural networks with computational

complexity analysis. *Computer Methods and Programs in Biomedicine*, 229:107277, 2023.

[25] UN DESA. United nations department of economic and social affairs, population division. world population prospects: The 2015 revision, key findings and advance tables. Technical report, Working Paper No. ESA/P/WP. 241, 2015.

[26] Usha Desai, Roshan Joy Martis, U Rajendra Acharya, C Gurudas Nayak, G Seshikala, and RANJAN SHETTY K. Diagnosis of multiclass tachycardia beats using recurrence quantification analysis and ensemble classifiers. *Journal of Mechanics in Medicine and Biology*, 16(01):1640005, 2016.

[27] Amit Dhurandhar, Karthikeyan Shanmugam, Ronny Luss, and Peder A Olsen. Improving simple models with confidence profiles. *Advances in Neural Information Processing Systems*, 31, 2018.

[28] Richard O Duda, Peter E Hart, David G Stork, et al. Pattern classification. *International Journal of Computational Intelligence and Applications*, 1:335–339, 2001.

[29] Athar A Ein Shoka, Monagi H Alkinani, AS El-Sherbeny, Ayman El-Sayed, and Mohamed M Dessouky. Automated seizure diagnosis system based on feature extraction and channel selection using eeg signals. *Brain Informatics*, 8(1):1–16, 2021.

[30] Oliver Faust, Yuki Hagiwara, Tan Jen Hong, Oh Shu Lih, and U Rajendra Acharya. Deep learning for healthcare applications based on physiological signals: a review. *Computer methods and programs in biomedicine*, 2018.

[31] Pedro J Freire, Sasipim Srivallapanondh, Antonio Napoli, Jaroslaw E Prilepsky, and Sergei K Turitsyn. Computational complexity evaluation of neural network applications in signal processing. *arXiv preprint arXiv:2206.12191*, 2022.

[32] Hamido Fujita and Dalibor Cimr. Computer aided detection for fibrillations and flutters using deep convolutional neural network. *Information Sciences*, 486, 2019.

[33] Hamido Fujita and Dalibor Cimr. Decision support system for arrhythmia prediction using convolutional neural network structure without preprocessing. *Applied Intelligence*, 49, 2019.

[34] Bin Gao, Jiazheng Zhou, Yuying Yang, Jinxin Chi, and Qi Yuan. Generative adversarial network and convolutional neural network-based eeg imbalanced classification model for seizure detection. *Biocybernetics and Biomedical Engineering*, 42(1):1–15, 2022.

[35] Shrimanti Ghosh, Ankur Banerjee, Nilanjan Ray, Peter W Wood, Pierre Boulanger, and Raj Padwal. Continuous blood pressure prediction from pulse transit time using ecg and ppg signals. In *2016 IEEE Healthcare Innovation Point-Of-Care Technologies Conference (HI-POCT)*, pages 188–191. IEEE, 2016.

[36] Ary L Goldberger, Luis AN Amaral, Leon Glass, Jeffrey M Hausdorff, Plamen Ch Ivanov, Roger G Mark, Joseph E Mietus, George B Moody, Chung-Kang Peng, and H Eugene Stanley. Physiobank, physiotoolkit, and physionet: components of a new research resource for complex physiologic signals. *circulation*, 101(23):e215–e220, 2000.

[37] JW Gordon. Certain molar movements of the human body produced by the circulation of the blood. *Journal of Anatomy and Physiology*, 11(Pt 3):533, 1877.

[38] Antonio Gulli and Sujit Pal. *Deep learning with Keras*. Packt Publishing Ltd, 2017.

[39] Yuki Hagiwara, Hamido Fujita, Shu Lih Oh, Jen Hong Tan, Ru San Tan, Edward J Ciaccio, and U Rajendra Acharya. Computer-aided diagnosis of atrial fibrillation based on ecg signals: a review. *Information Sciences*, 467:99–114, 2018.

[40] Ibrahim Hamed and Mohamed I Owis. Automatic arrhythmia detection using support vector machine based on discrete wavelet transform. *Journal of Medical Imaging and Health Informatics*, 6(1):204–209, 2016.

[41] Ahnaf Rashik Hassan. Computer-aided obstructive sleep apnea detection using normal inverse gaussian parameters and adaptive boosting. *Biomedical Signal Processing and Control*, 29:22–30, 2016.

[42] Kaiming He, Xiangyu Zhang, Shaoqing Ren, and Jian Sun. Deep residual learning for image recognition. In *Proceedings of the IEEE conference on computer vision and pattern recognition*, pages 770–778, 2016.

[43] Andrew G Howard, Menglong Zhu, Bo Chen, Dmitry Kalenichenko, Weijun Wang, Tobias Weyand, Marco Andreetto, and Hartwig Adam. Mobilenets: Efficient convolu-

tional neural networks for mobile vision applications. *arXiv preprint arXiv:1704.04861*, 2017.

[44] Gao Huang, Zhuang Liu, Laurens Van Der Maaten, and Kilian Q Weinberger. Densely connected convolutional networks. In *Proceedings of the IEEE conference on computer vision and pattern recognition*, pages 4700–4708, 2017.

[45] Su Hwan Hwang, Yu Jin Lee, Do-Un Jeong, Kwang Suk Park, et al. Oxygen desaturation index estimation through unconstrained cardiac sympathetic activity assessment using three ballistocardiographic systems. *Respiration*, 92(2):90–97, 2016.

[46] Omer T Inan, Pierre-Francois Migeotte, Kwang-Suk Park, Mozziyar Etemadi, Kouhyar Tavakolian, Ramon Casanella, John Zanetti, Jens Tank, Irina Funtova, G Kim Prisk, et al. Ballistocardiography and seismocardiography: A review of recent advances. *IEEE journal of biomedical and health informatics*, 19(4):1414–1427, 2015.

[47] Hao-Yu Jan, Mei-Fen Chen, Tieh-Cheng Fu, Wen-Chen Lin, Cheng-Lun Tsai, and Kang-Ping Lin. Evaluation of coherence between ecg and ppg derived parameters on heart rate variability and respiration in healthy volunteers with/without controlled breathing. *Journal of Medical and Biological Engineering*, 39(5):783–795, 2019.

[48] Craig T January, L Samuel Wann, Joseph S Alpert, Hugh Calkins, Joaquin E Cigarroa, Jamie B Conti, Patrick T Ellinor, Michael D Ezekowitz, Michael E Field, Katherine T Murray, et al. 2014 aha/acc/hrs guideline for the management of patients with atrial fibrillation: a report of the american college of cardiology/american heart association task force on practice guidelines and the heart rhythm society. *Journal of the American College of Cardiology*, 64(21):e1–e76, 2014.

[49] Muhammad Umar Khan, Sumair Aziz, Muhammad Bilal, and Muhammad Bilal Aamir. Classification of emg signals for assessment of neuromuscular disorder using empirical mode decomposition and logistic regression. In *2019 International Conference on Applied and Engineering Mathematics (ICAEM)*, pages 237–243. IEEE, 2019.

[50] Hamid Khorrami and Majid Moavenian. A comparative study of dwt, cwt and dct transformations in ecg arrhythmias classification. *Expert systems with Applications*, 37(8):5751–5757, 2010.

[51] Yoon Kim. Convolutional neural networks for sentence classification. *arXiv preprint arXiv:1408.5882*, 2014.

[52] Jan Kříž and Petr Šeba. Force plate monitoring of human hemodynamics. *Nonlinear biomedical physics*, 2(1):1, 2008.

[53] Thomas Kurian, Christina Ambrosi, William Hucker, Vadim V Fedorov, and Igor R Efimov. Anatomy and electrophysiology of the human av node. *Pacing and Clinical Electrophysiology*, 33(6):754–762, 2010.

[54] Yann LeCun, Yoshua Bengio, et al. Convolutional networks for images, speech, and time series. *The handbook of brain theory and neural networks*, 3361(10):1995, 1995.

[55] Erich L Lehmann and Joseph P Romano. *Testing statistical hypotheses*. Springer Science & Business Media, 2006.

[56] Chaosong Li, Weidong Zhou, Guoyang Liu, Yanli Zhang, Minxing Geng, Zhen Liu, Shang Wang, and Wei Shang. Seizure onset detection using empirical mode decomposition and common spatial pattern. *IEEE Transactions on Neural Systems and Rehabilitation Engineering*, 29:458–467, 2021.

[57] Mingyang Li, Xiaoying Sun, and Wanzhong Chen. Patient-specific seizure detection method using nonlinear mode decomposition for long-term eeg signals. *Medical & Biological Engineering & Computing*, 58(12):3075–3088, 2020.

[58] Mingyang Li, Wanzhong Chen, and Min Xia. Gnmf-based quadratic feature extraction in sstft domain for epileptic eeg detection. *Biomedical Signal Processing and Control*, 80:104274, 2023.

[59] Fan Liu, Xingshe Zhou, Zhu Wang, Tianben Wang, Hongbo Ni, and Jun Yang. Identifying obstructive sleep apnea by exploiting fine-grained bcg features based on event phase segmentation. In *Bioinformatics and Bioengineering (BIBE), 2016 IEEE 16th International Conference on*, pages 293–300. IEEE, 2016.

[60] Badreddine Mandhouj, Mohamed Ali Cherni, and Mounir Sayadi. An automated classification of eeg signals based on spectrogram and cnn for epilepsy diagnosis. *Analog Integrated Circuits and Signal Processing*, 108(1):101–110, 2021.

[61] Juan Pablo Martínez, Rute Almeida, Salvador Olmos, Ana Paula Rocha, and Pablo Laguna. A wavelet-based ecg delineator: evaluation on standard databases. *IEEE Transactions on biomedical engineering*, 51(4):570–581, 2004.

[62] Roshan Joy Martis, U Rajendra Acharya, Hojjat Adeli, Hari Prasad, Jen Hong Tan, Kuang Chua Chua, Chea Loon Too, Sharon Wan Jie Yeo, and Louis Tong. Computer aided diagnosis of atrial arrhythmia using dimensionality reduction methods on transform domain representation. *Biomedical signal processing and control*, 13:295–305, 2014.

[63] A Muthuchudar and Lt Dr S Santosh Baboo. A study of the processes involved in ecg signal analysis. *International Journal of Scientific and Research Publications*, 3(3):1–5, 2013.

[64] Yoko Nagai, Christopher Iain Jones, and Arjune Sen. Galvanic skin response (gsr)/electrodermal/skin conductance biofeedback on epilepsy: a systematic review and meta-analysis. *Frontiers in neurology*, 10:377, 2019.

[65] Samaneh Nasiri and Gari D Clifford. Generalizable seizure detection model using generating transferable adversarial features. *IEEE Signal Processing Letters*, 28:568–572, 2021.

[66] Andrea Natale, Antonio Raviele, AMIN AL-AHMAD, Ottavio Alfieri, Etienne Aliot, Jesus Almendral, GÜnter Breithardt, Josep Brugada, Hugh Calkins, David Callans, et al. Venice chart international consensus document on ventricular tachycardia/ventricular fibrillation ablation. *Journal of cardiovascular electrophysiology*, 21(3):339–379, 2010.

[67] David Orlikowski, Helene Prigent, Maria-Antonia Quera Salva, Nicholas Heming, Cendrine Chaffaut, Sylvie Chevret, Djillali Annane, Frederic Lofaso, and Adam Ogna. Prognostic value of nocturnal hypoventilation in neuromuscular patients. *Neuromuscular Disorders*, 27(4):326–330, 2017.

[68] Yüksel Özbay, Rahime Ceylan, and Bekir Karlik. Integration of type-2 fuzzy clustering and wavelet transform in a neural network based ecg classifier. *Expert Systems with Applications*, 38(1):1004–1010, 2011.

[69] Saurabh Pal and Madhuchhanda Mitra. Empirical mode decomposition based ecg enhancement and qrs detection. *Computers in biology and medicine*, 42(1):83–92, 2012.

[70] Eduardo Pinheiro, Octavian Postolache, and Pedro Girão. Non-intrusive device for real-time circulatory system assessment with advanced signal processing capabilities. *Measurement Science Review*, 10(5):166–175, 2010.

[71] Sai Manoj Pudukotai Dinakarrao and Axel Jantsch. Addhard: Arrhythmia detection with digital hardware by learning ecg signal. In *Proceedings of the 2018 on Great Lakes Symposium on VLSI*, pages 495–498. ACM, 2018.

[72] Saeed Mian Qaisar and Syed Fawad Hussain. Effective epileptic seizure detection by using level-crossing eeg sampling sub-bands statistical features selection and machine learning for mobile healthcare. *Computer Methods and Programs in Biomedicine*, 203: 106034, 2021.

[73] Faisal Rahman, Na Wang, Xiaoyan Yin, Patrick T Ellinor, Steven A Lubitz, Paul A LeLorier, David D McManus, Lisa M Sullivan, Sudha Seshadri, Ramachandran S Vasan, et al. Atrial flutter: clinical risk factors and adverse outcomes in the framingham heart study. *Heart Rhythm*, 13(1):233–240, 2016.

[74] B Banu Rekha, A Kandaswamy, and RMPL Ramanathan. Ensemble classification approach for screening of obstructive sleep apnoea using ecg. *International Journal of Biomedical Engineering and Technology*, 27(1-2):139–150, 2018.

[75] Sebastian Ruder. An overview of gradient descent optimization algorithms. *arXiv preprint arXiv:1609.04747*, 2016.

[76] Ibrahim Sadek, Edwin Seet, Jit Biswas, Bessam Abdulrazak, and Mounir Mokhtari. Nonintrusive vital signs monitoring for sleep apnea patients: A preliminary study. *IEEE Access*, 6:2506–2514, 2018.

[77] Muhammad Tariq Sadiq, Muhammad Zulkifal Aziz, Ahmad Almogren, Adnan Yousaf, Siuly Siuly, and Ateeq Ur Rehman. Exploiting pretrained cnn models for the development of an eeg-based robust bci framework. *Computers in Biology and Medicine*, 143: 105242, 2022.

[78] Milad Salem, Shayan Taheri, and Jiann-Shiun Yuan. Ecg arrhythmia classification using transfer learning from 2-dimensional deep cnn features. In *2018 IEEE Biomedical Circuits and Systems Conference (BioCAS)*, pages 1–4. IEEE, 2018.

[79] Mark E Silverman and J Willis Hurst. Willem einthoven—the father of electrocardiography. *Clinical cardiology*, 15(10):785–787, 1992.

[80] Miguel Simão, Nuno Mendes, Olivier Gibaru, and Pedro Neto. A review on electromyography decoding and pattern recognition for human-machine interaction. *Ieee Access*, 7:39564–39582, 2019.

[81] Karen Simonyan and Andrew Zisserman. Very deep convolutional networks for large-scale image recognition. *arXiv preprint arXiv:1409.1556*, 2014.

[82] Filip Studnicka. Ballistocardiography with breathing disorderes, 2020. Mendeley Data, v1, `https://data.mendeley.com/datasets/9fmfn6kfn7/1`.

[83] Christian Szegedy, Wei Liu, Yangqing Jia, Pierre Sermanet, Scott Reed, Dragomir Anguelov, Dumitru Erhan, Vincent Vanhoucke, and Andrew Rabinovich. Going deeper with convolutions. In *Proceedings of the IEEE conference on computer vision and pattern recognition*, pages 1–9, 2015.

[84] Hui-Leng Tan, Leila Kheirandish-Gozal, François Abel, and David Gozal. Craniofacial syndromes and sleep-related breathing disorders. *Sleep medicine reviews*, 27:74–88, 2016.

[85] Roland D Thijs, Rainer Surges, Terence J O'Brien, and Josemir W Sander. Epilepsy in adults. *The Lancet*, 393(10172):689–701, 2019.

[86] Wei-Chieh Tseng, Mei-Hwan Wu, Hui-Chi Chen, Feng-Yu Kao, and San-Kuei Huang. Ventricular fibrillation in a general population–a national database study–. *Circulation Journal*, 80(11):2310–2316, 2016.

[87] Elif Derya Übeyli. Ecg beats classification using multiclass support vector machines with error correcting output codes. *Digital Signal Processing*, 17(3):675–684, 2007.

[88] Antti Vehkaoja, Anton Kontunen, and Jukka Lekkala. Effects of sensor type and sensor location on signal quality in bed mounted ballistocardiographic heart rate and respi-

ration monitoring. In *Engineering in Medicine and Biology Society (EMBC), 2015 37th Annual International Conference of the IEEE*, pages 4383–4386. IEEE, 2015.

[89] Albert L Waldo. Atrial fibrillation and atrial flutter: Two sides of the same coin! *International journal of cardiology*, 240:251–252, 2017.

[90] Albert L Waldo and Gregory K Feld. Inter-relationships of atrial fibrillation and atrial flutter: mechanisms and clinical implications. *Journal of the American College of Cardiology*, 51(8):779–786, 2008.

[91] Lei Wang, Xi Long, Ronald M Aarts, Johannes P van Dijk, and Johan BAM Arends. Eeg-based seizure detection in patients with intellectual disability: Which eeg and clinical factors are important? *Biomedical Signal Processing and Control*, 49:404–418, 2019.

[92] Xiaoshuang Wang, Xiulin Wang, Wenya Liu, Zheng Chang, Tommi Kärkkäinen, and Fengyu Cong. One dimensional convolutional neural networks for seizure onset detection using long-term scalp and intracranial eeg. *Neurocomputing*, 459:212–222, 2021.

[93] Xiashuang Wang, Guanghong Gong, Ni Li, and Shi Qiu. Detection analysis of epileptic eeg using a novel random forest model combined with grid search optimization. *Frontiers in human neuroscience*, 13:52, 2019.

[94] Zuochen Wei, Junzhong Zou, Jian Zhang, and Jianqiang Xu. Automatic epileptic eeg detection using convolutional neural network with improvements in time-domain. *Biomedical Signal Processing and Control*, 53:101551, 2019.

[95] William Wenger and Paul Kligfield. Variability of precordial electrode placement during routine electrocardiography. *Journal of electrocardiology*, 29(3):179–184, 1996.

[96] Hugh Williams. Geometric methods and applications for computer science and engineering, by jean gallier. pp. 572.£ 44.50. 2001. isbn 0 387 95044 3 (springer-verlag). *The Mathematical Gazette*, 86(507):564–565, 2002.

[97] Herbert Witte, Leon D Iasemidis, and Brian Litt. Special issue on epileptic seizure prediction. *IEEE transactions on biomedical engineering*, 50(5):537–539, 2003.

[98] Yong Xia, Naren Wulan, Kuanquan Wang, and Henggui Zhang. Detecting atrial fibrillation by deep convolutional neural networks. *Computers in biology and medicine*, 93:84–92, 2018.

[99] Xiaomin Xu and Ying Liu. Ecg qrs complex detection using slope vector waveform (svw) algorithm. In *Engineering in Medicine and Biology Society, 2004. IEMBS'04. 26th Annual International Conference of the IEEE*, volume 2, pages 3597–3600. IEEE, 2004.

[100] Yu Yao, Christoph Bruser, Uwe Pietrzyk, Steffen Leonhardt, Stefan van Waasen, and Michael Schiek. Model-based verification of a non-linear separation scheme for ballistocardiography. *IEEE journal of biomedical and health informatics*, 18(1):174–182, 2014.

[101] Chan Yuan, Yan Yan, Lin Zhou, Jingwen Bai, and Lei Wang. Automated atrial fibrillation detection based on deep learning network. In *Information and Automation (ICIA), 2016 IEEE International Conference on*, pages 1159–1164. IEEE, 2016.

[102] Ye Yuan, Guangxu Xun, Kebin Jia, and Aidong Zhang. A multi-view deep learning framework for eeg seizure detection. *IEEE journal of biomedical and health informatics*, 23(1):83–94, 2018.

[103] Morteza Zabihi, Serkan Kiranyaz, Ville Jäntti, Tarmo Lipping, and Moncef Gabbouj. Patient-specific seizure detection using nonlinear dynamics and nullclines. *IEEE journal of biomedical and health informatics*, 24(2):543–555, 2019.

[104] Asghar Zarei and Babak Mohammadzadeh Asl. Automatic seizure detection using orthogonal matching pursuit, discrete wavelet transform, and entropy based features of eeg signals. *Computers in Biology and Medicine*, 131:104250, 2021.

[105] Tong Zhang, Wenming Zheng, Zhen Cui, Yuan Zong, and Yang Li. Spatial–temporal recurrent neural network for emotion recognition. *IEEE transactions on cybernetics*, 49(3):839–847, 2018.

[106] Weichao Zhao, Hongbo Ni, Xingshe Zhou, Yalong Song, and Tianben Wang. Identifying sleep apnea syndrome using heart rate and breathing effort variation analysis based on ballistocardiography. In *Engineering in Medicine and Biology Society (EMBC), 2015 37th Annual International Conference of the IEEE*, pages 4536–4539. IEEE, 2015.

[107] Matthias Daniel Zink, Christoph Brüser, Björn-Ole Stüben, Andreas Napp, Robert Stöhr, Steffen Leonhardt, Nikolaus Marx, Karl Mischke, Jörg B Schulz, and Johannes Schiefer. Unobtrusive nocturnal heartbeat monitoring by a ballistocardiographic sensor in patients with sleep disordered breathing. *Scientific Reports*, 7(1):13175, 2017.

[108] Barret Zoph, Vijay Vasudevan, Jonathon Shlens, and Quoc V Le. Learning transferable architectures for scalable image recognition. In *Proceedings of the IEEE conference on computer vision and pattern recognition*, pages 8697–8710, 2018.

Author's publication in an IF or SJR journal

Dalibor Cimr and Filip Studnička. Automatic detection of breathing disorder from ballistocardiography signals. *Knowledge-Based Systems*, 188, 2020.

Dalibor Cimr, Filip Studnicka, Hamido Fujita, Hana Tomaskova, Richard Cimler, Jitka Kuhnova, and Jan Slegr. Computer aided detection of breathing disorder from ballistocardiography signal using convolutional neural network. *Information Sciences*, 541, 2020.

Dalibor Cimr, Filip Studnicka, Hamido Fujita, Richard Cimler, and Jan Slegr. Application of mechanical trigger for unobtrusive detection of respiratory disorders from body recoil micro-movements. *Computer Methods and Programs in Biomedicine*, 207, 2021.

Dalibor Cimr, Hamido Fujita, Hana Tomaskova, Richard Cimler, and Ali Selamat. Automatic seizure detection by convolutional neural networks with computational complexity analysis. *Computer Methods and Programs in Biomedicine*, 229:107277, 2023.

Hamido Fujita and Dalibor Cimr. Computer aided detection for fibrillations and flutters using deep convolutional neural network. *Information Sciences*, 486, 2019.

Hamido Fujita and Dalibor Cimr. Decision support system for arrhythmia prediction using convolutional neural network structure without preprocessing. *Applied Intelligence*, 49, 2019.

Toshitaka Hayashi, Dalibor Cimr, Filip Studnička, Hamido Fujita, and Damián Bušovskỳ. OCSTN: One-class time-series classification approach using a signal transformation network into a goal signal. *Information Sciences*, 614, 2022.

Author's publication in the conference's indexed proceedings

Richard Cimler, Dalibor Cimr, Jitka Kuhnova, and Hana Tomaskova. Novel effective algorithm for synchronization problem in directed graph. In *International Conference on Computational Collective Intelligence*, pages 528–537. Springer, 2017.

Dalibor Cimr and Josef Hynek. Heuristic algorithm for a personalised student timetable. In *International Conference on Computational Collective Intelligence*, pages 79–88. Springer, 2018.

Dalibor Cimr, Richard Cimler, and Hana Tomášková. Combination of collision detection and visibility algorithms in simulation of the effective placement of anti-air elements. In *Asian Conference on Intelligent Information and Database Systems*, pages 213–221. Springer, 2017.

Dalibor Cimr, Hana Tomaskova, Richard Cimler, Jitka Kuhnova, and Vlastimil Slouf. A system to evaluate an air-strike threat level using fuzzy methods. In *International Conference on Computational Collective Intelligence*, pages 322–331. Springer, 2018.

T. Hayashi, D. Cimr, and R. Cimler. Image entropy equalization for autoencoder-based one-class classification. In *Frontiers in Artificial Intelligence and Applications*, pages 310–321, 2022.

David Sec, Dalibor Cimr, Jan Stepan, Richard Cimler, and Jitka Kuhnova. Automatic address assigning problem in smart homes. In *2018 IEEE International Conference on Fuzzy Systems (FUZZ-IEEE)*, pages 1–6. IEEE, 2018.

David Sec, Dalibor Cimr, Jan Stepan, Richard Cimler, and Jitka Kuhnova. Optimized algorithm for node address assigning in a large-scale smart automation environment. In *International Conference on Computational Collective Intelligence*, pages 311–321. Springer, 2018.

A summary of the author's published works and project collaborations

A summary of the author's published works:

	No. publications	h-index	No. citations
WoS	14	4	168
Scopus	15	5	190
Google Scholar	14	6	224

A summary of the author's peer review:

Journal	No. revisions	IF 2021	IF quartile	AIS quartile
Applied Intelligence	16	5.019	Q2	Q2
Knowledge-Based Systems	12	8.139	Q1	Q1
Artificial Intelligence in Medicine	5	7.011	Q1	Q1
Journal of King Saud University	3	8.839	Q1	Q1
IEEE Sensors Journal	1	4.325	Q1	Q2
Scientific Reports	1	4.996	Q2	Q1

Participation in projects:

Czech Science Foundation (GAČR)

18-01246SS	Member	Non-standard optimisation and decision-making methods in management processes

Excelence

2016	Member	Simulation of migration theories – SioMiTe
2017	Member	Optimization and Multiagent Models 4 - OPTIMAM 4
2019	Member	Decision Support Systems: Principles and Applications

Specific Research (SPEV)

2017	Member	Autonomous socio-economic systems
2018	Member	Computer networks for the cloud, distributed computing, and the Internet of Things
2018	Member	Socio-economic models
2019	Member	Computer networks for the cloud, distributed computing, and the Internet of Things II